Available online at www.sciencedirect.com
ScienceDirect
Earth and Planetary Science Letters 263 (2007) 288–308
EPSL
www.elsevier.com/locate/epsl

Primary Carboniferous and Permian paleomagnetic results from the Yili Block (NW China) and their implications on the geodynamic evolution of Chinese Tianshan Belt

Bo Wang [a,b,*], Yan Chen [b], Sheng Zhan [b,c], Liangshu Shu [a], Michel Faure [b], Dominique Cluzel [b], Jacques Charvet [b], Sébastien Laurent-Charvet [d]

[a] *Department of Earth Sciences, Nanjing University, 210093, Nanjing, China*
[b] *Institut des Sciences de la Terre d'Orléans, UMR CNRS 6113, Université d'Orléans, 45067, Orléans, France*
[c] *Key Laboratory of Orogenic Belts and Crustal Evolution, Peking University, 100871, Beijing, China*
[d] *Institut Géologique Albert-de-Lapparent, 95092, Cergy-Pontoise, France*

Received 28 July 2006; received in revised form 19 April 2007; accepted 27 August 2007
Available online 18 September 2007
Editor: C.P. Jaupart

Abstract

In order to better understand the tectonic role of the Yili Block on the Paleozoic evolution of the Chinese Tianshan Belt, we performed a primary paleomagnetic study on Carboniferous and Permian rocks from different areas in the Yili Block, NW of China. More than 320 sedimentary and volcanic samples were collected from 39 sites. Except for the Ordovician samples showing a weak and unstable magnetic remanence, the majority of this collection presents characteristic remanent magnetization carried by magnetite and hematite. In the study area, though positive fold test has been observed on the Early Carboniferous rocks, a general re-magnetization of these rocks has been identified and attributed to the Late Carboniferous magmatism. Moreover, all Early and Late Carboniferous samples from the interior of the Yili Block yield stable and coherent magnetic directions with exhaustively reverse magnetic polarity. The Late Carboniferous (C_2) is considered as the magnetic remanence age since these rocks are covered or intruded by synchronous magmatic rocks of the Yili arc, which lasted until to ~310 Ma. The C_2 paleomagnetic pole is therefore calculated at 68.6°N, 290.6°E with $A_{95}=6.4°$ and $n=15$. The Late Carboniferous rocks located close to a deformation zone present a consistent magnetic inclination but significant different declination with respect to other areas and are suspected to have probably experienced a local rotation. Although no fold test can be performed due to the monoclinal bedding, stable magnetic components are isolated from Late Permian (P_2) red beds in the interior of the Yili Block with also a solo reverse magnetic polarity, the P_2 paleomagnetic pole of the Yili Block has been, therefore, calculated from the characteristic remanent magnetization: 79.7°N, 172.0°E with $A_{95}=11.3°$ and $n=5$. Keeping important uncertainties in mind, comparisons of the C_2 and P_2 paleomagnetic poles of the Yili Block with available coeval poles of Junggar, Tarim and Siberia indicate (1) no significant relative motion between the Yili and Junggar blocks since the Late Carboniferous, (2) no significant or weak latitudinal relative motion occurred since the Late Carboniferous among these blocks, but (3) the 46.2°±15.1° and the 31.6°±15.1° counterclockwise rotations of the Yili–Junggar blocks with respect to Tarim and Siberia took place during C_2 to P_2. These rotations are accommodated by the Permian dextral

* Corresponding author. Department of Earth Sciences, Nanjing University, 210093, Nanjing, China. Tel.: +86 25 8359 2921; fax: +86 25 8368 6061.
E-mail addresses: wangbo1996@nju.org.cn, bo.wang@univ-orleans.fr (B. Wang).

0012-821X/$ - see front matter © 2007 Published by Elsevier B.V.
doi:10.1016/j.epsl.2007.08.037

strike–slip faults along the northern and southern sides of Tianshan Belt and sinistral strike–slip faulting along the Erqishi Fault of Altay Belt, resulting in about 1000 km and 600 km lateral displacements in the Tianshan and Altay belts, respectively.

Keywords: Yili Block; Tianshan Belt; Paleozoic; paleomagnetism; rotation; strike–slip faulting

1. Introduction

The "Yili Block" represents a triangular shape sandwiched within the Tianshan Belt and widening westwards into Kazakhstan and Kyrgyzstan (Fig. 1a; Enkin et al., 1991). It is considered as a microcontinent with a Precambrian basement separating the Tianshan Belt into northern and southern branches (Allen et al., 1992; Chen et al., 1999; Wang et al., 2006, 2007). The Yili Block, therefore, occupies an important position for the understanding of the tectonic evolution of the Tianshan Belt. It is widely accepted that the Tianshan Belt is a Paleozoic orogenic belt due to multi-phase accretion and amalgamation of various microcontinents, and magmatic arcs (Coleman, 1989; Shi et al., 1994; Shu et al., 2000, 2002). However, there are still controversies on procedures of amalgamation and chronological constraints. The Paleozoic Tianshan Belt is considered to be formed by subduction–collision processes (Windley et al., 1990; Allen et al., 1992; Gao et al., 1998; Chen et al., 1999), i.e. the Yili Block and the Central Tianshan microcontinents (Fig. 1b) were rifted from the Tarim Plate in the Cambrian, and were reaccreted to Tarim during Ordovician to Early Carboniferous due to the multi-phase subduction of oceanic crust. A southward subduction of an oceanic crust beneath the Yili Block during the Late Devonian to the Late Carboniferous terminated the convergent phases of mountain building in the Tianshan Belt. Nevertheless, some authors considered the Tianshan Belt as a part of the Altaids, which was mainly produced by strike–slip faulting (Sengör et al., 1993; Sengör and Natal'in, 1996). Recently, some workers suggested that an oceanic crust existed in the southern Tianshan until the end of Permian on the basis of radiolarians found in South Tianshan ophiolitic mélange (Li et al., 2002, 2005). Besides, a Late Carboniferous to Early Permian continental rifting is also proposed according to geochemical and isotopic studies on the volcanic rocks in the Tianshan Belt (Xia et al., 2004). These results suggest a divergent tectonics and a subsequent renewed convergence in the Tianshan area from Carboniferous to Permian, and therefore arise a controversy on the final evolution of the Tianshan Belt.

In addition, Permian transcurrent faulting is widely observed, especially ductile strike–slip faults are geologically well documented in the whole northern Xinjiang area (Allen et al., 1995; Shu et al., 1999; Laurent-Charvet et al., 2002, 2003; Wang et al., 2006), including two main dextral strike–slip faults along the northern and the southern sides of the Tianshan Belt, and a sinistral strike–slip fault, the Erqishi Fault, in the Altay Belt. However, the southern fault of the Tianshan Belt was previously interpreted as a sinistral strike–slip fault (Sengör et al., 1993; Burtman, 1975), which is also suggested on the basis of a significant westward deflection of magnetic declination (Bazhenov et al., 1993, 1999), but this is not consistent with the geological and kinematic observations from Chinese Tianshan area (Yin and Nie, 1996; Wang et al., in review), where no paleomagnetic data are available up to now to constrain this event and consequent lateral displacement.

In order to improve the understanding of the final orogenic procedures, this paleomagnetic study was carried out on Ordovician to Permian rocks from the Yili Block. The comparison of paleomagnetic data from this study with the previous results from Junggar, Tarim and Siberia blocks will better constrain the tectonic evolution of the Chinese Tianshan Belt during the Late Paleozoic time.

2. Geological setting and paleomagnetic sampling

The Western Chinese Tianshan Belt is divided into several subunits, namely North Tianshan domain, Bole Block, Yili Block, Central Tianshan domain and South Tianshan mélange zone (Fig. 1b). In the Yili Block, the Precambrian basement is composed of Meso- to Neoproterozoic carbonates, clastic rocks and amphibolite facies metamorphic rocks developing along its northern and southern boundaries (XBGMR, 1993; Chen et al., 2000). Early Paleozoic rocks consist of Cambrian to Ordovician carbonates and clastic rocks, and Silurian flysch in north of Yining area (Fig. 2a). The Devonian is mainly represented by terrigeneous rocks and arc-derived granitoids.

The Lower Carboniferous is, a ca. 3500 m-thick series of limestone, sandstone and shale with subordinate volcanic rocks, and the Upper Carboniferous consists of limestone intercalated with volcanoclastic sandstone and massive volcanic rocks (Fig. 2). Both Lower and Upper Carboniferous rocks are coeval with granitoids. Several geochronological studies on the volcanic and granitic rocks provide zircon U–Pb (SHRIMP and LA-ICPMS)

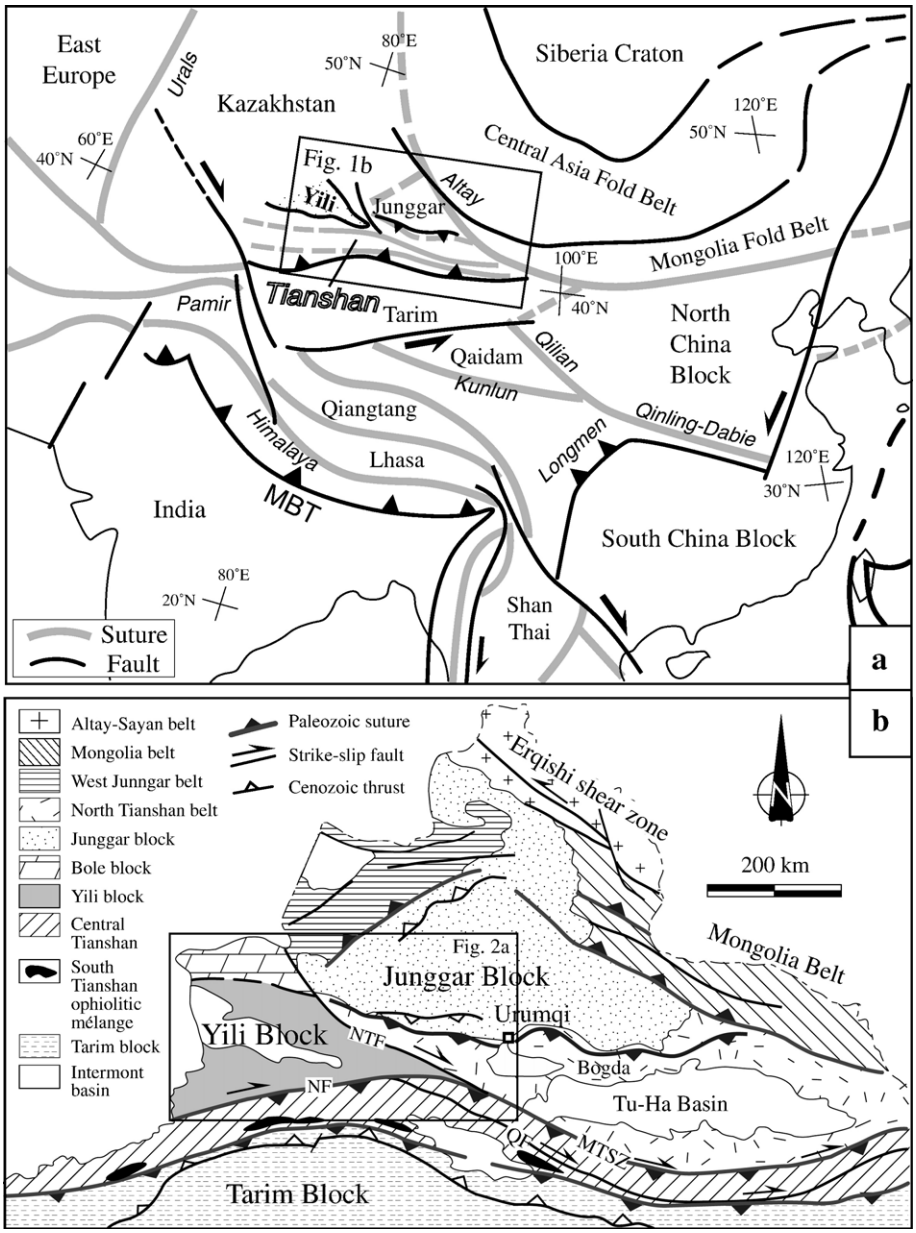

Fig. 1. (a) Tectonic sketch map of Central Asia (modified after Enkin et al., 1991) showing the main tectonic blocks including the Yili Block, (b) structural map of Chinese Tianshan Belt and its adjacent areas. Paleozoic sutures, Permian strike–slip faults and Cenozoic thrusts are shown. Abbreviations: NTF, North Tianshan Fault; NF, Nalati Fault; MTSZ, Main Tianshan Shear Zone; QF, Qingbulake Fault.

ages ranging from 361 Ma to 309 Ma (Zhu et al., 2005; Wang et al., 2006). Geochemical and isotopic studies suggest that the Yili Block was an active continental margin during the Late Devonian to Late Carboniferous (Zhu et al., 2005; Wang et al., 2007).

In the whole Western Chinese Tianshan Belt, Permian terrestrial sandstone and conglomerate unconformably overlie the older rocks (Fig. 2). Lower to Upper Permian bimodal volcanic and plutonic rocks are widespread throughout the Yili Block but form small occurrences (Fig. 2a; XBGMR, 1993; Allen et al., 1995; Zhou et al., 2001; Shu et al., 2005). Strike–slip shear faults overprinted the Paleozoic sutures during Permian and underwent multi-phase reactivation during the early Mesozoic (Shu et al., 1999; Laurent-Charvet et al., 2002, 2003; Shu et al., 2003). The Tianshan Belt is reactivated again by the Cenozoic intra-continental deformation and subsequently uplifted in response to

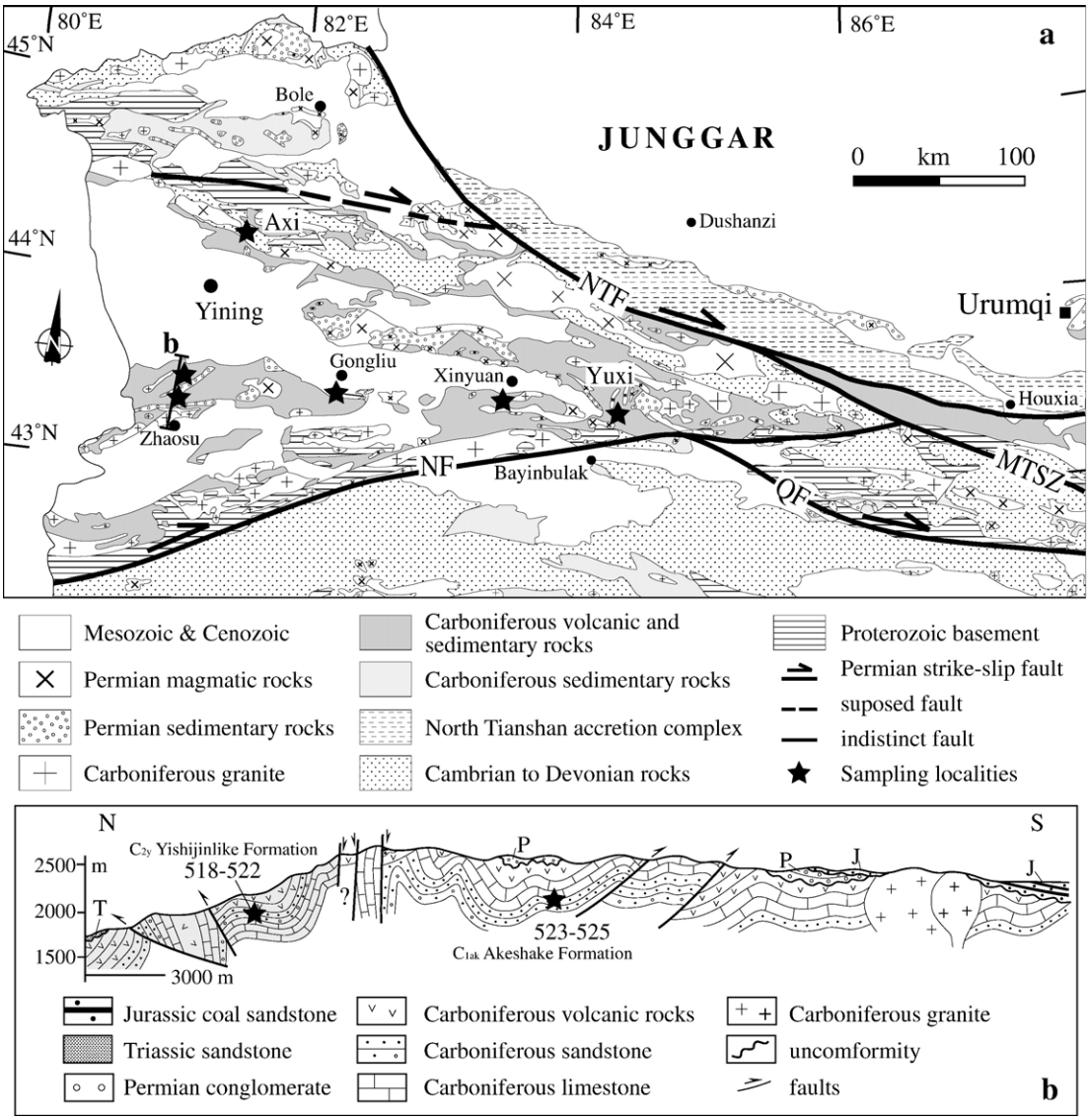

Fig. 2. (a) Geological map of the Yili Block and adjacent areas indicating the sampling localities, (b) simplified cross section of Zhaosu area.

the India–Asia collision (Tapponnier and Molnar, 1979; Avouac et al., 1993; Burchfiel et al., 1999; Shu et al., 2003; Charreau et al., 2005).

In the Yili Block, more than 320 cores of 39 sites were paleomagnetically sampled from 5 localities (Fig. 2a; Table 1). Ordovician sandstone and pelitic limestone were collected from Axi section (Fig. 2a). Early to Late Carboniferous red sandstone, volcanoclastic sandstone, basalt and andesite were collected from Zhaosu, Xinyuan and Yuxi areas. In basalt and andesite that are exposed as massive rocks, the layering (initial horizontal surface) was estimated from the underlying or overlying sedimentary rocks. Late Permian red beds were collected from the Gongliu area. Detailed sampling information may be found in Table 1. Depending on strata thickness, 6 to 12 cores were drilled from each site with a portable gasoline drill. Each core was orientated by both magnetic and solar compasses, when it was possible. The average of differences between these two azimuths is about 4.0°±3.4°, and this value was used for the orientation corrections to those samples measured only by magnetic compass as well as for the trends of bedding.

3. Laboratory methods

Several methods were applied to magnetic mineralogical investigations: thermal magnetic (Curie point)

Table 1
Paleomagnetic sampling and measurement results from the Yili Block

Site	Coordinates	Rocks	Age	Strike/dip	n/N[a]	P	Dg	Ig	Ds	Is	k	α_{95}
Zhaosu area												
523	43.3°N, 81.0°E	Andesitic sandstone	$C_1ak(C_2)$[b]	110/12	6/8	R	185.1	−43.5	181.1	−55.0	140.7	6.5
524	43.3°N, 81.0°E	Red sandstone	$C_1ak(C_2)$	245/25	6/8	R	190.4	−63.0	174.0	−40.3	354.9	3.2
525	43.3°N, 81.0°E	Sandstone	$C_1ak(C_2)$	255/26	6/9	R	184.0	−63.7	176.1	−38.4	324.7	3.7
526	43.3°N, 81.6°E	Yellow sandstone	$C_1ak(C_2)$	230/78	7/10	R	258.6	−41.8	188.6	−29.2	220.0	4.1
Mean					4	R	207.3	−57.8			10.5	29.8
									180.2	−40.9	46.9	13.6
518	43.5°N, 81.1°E	Red sandstone	C_{2y}	270/18	6/8	R	153.1	−61.8	163.1	−45.3	197.6	4.8
519	43.5°N, 81.1°E	Red sandstone	C_{2y}	305/22	6/8	R	116.3	−57.5	149.0	−54.0	66.7	6.0
520	43.4°N, 81.1°E	Sandstone	C_{2y}	270/20	6/10	R	169.1	−57.2	179.0	−39.1	43.1	9.3
521	43.4°N, 81.1°E	Sandstone	C_{2y}	280/15	6/8	R	171.6	−57.9	176.4	−43.4	84.4	7.3
522	43.4°N, 81.1°E	Sandstone	C_{2y}	250/12	6/9	R	145.7	−63.5	149.7	−51.8	80.4	6.2
Mean					5	R	151.6	−61.2			48.0	11.2
									164.7	−47.4	50.7	10.9
Xinyuan area												
532	43.3°N, 83.3°E	Tuffaceous sandstone	C_1aw	287/48	9/9	–	–	–	–	–	–	–
533	43.3°N, 83.3°E	Tuffaceous sandstone	C_1aw	285/51	8/8	–	–	–	–	–	–	–
534	43.3°N, 83.3°E	Tuffaceous sandstone	C_1aw	292/52	8/9	–	–	–	–	–	–	–
535	43.3°N, 83.3°E	Tuffaceous sandstone	C_1aw	268/45	8/8	–	–	–	–	–	–	–
536	43.3°N, 83.3°E	Tuffaceous sandstone	C_1aw	272/48	9/9	–	–	–	–	–	–	–
537	43.3°N, 83.3°E	Basalt	$C_1aw(C_2)$	240/47	7/9	R	181.5	−24.0	179.9	16.9	6.1	21.2
538	43.3°N, 83.3°E	Basaltic tuff	$C_1aw(C_2)$	237/49	8/8	R	167.9	−27.4	166.6	18.9	35.9	7.7
539	43.3°N, 83.3°E	Basalt	$C_1aw(C_2)$	237/49	8/8	R	156.2	−30.5	155.4	18.0	11.2	14.3
540	43.3°N, 83.3°E	Basalt	$C_1aw(C_2)$	237/49	8/12	R	160.5	−36.6	216.7	−64.4	35.0	7.8
541	43.4°N, 83.3°E	Rhyolitic sandstone	$C_1aw(C_2)$	38/48	6/7	R	149.0	−5.2	160.8	−48.7	289.7	3.9
542	43.4°N, 83.3°E	Rhyolitic sandstone	$C_1aw(C_2)$	29/47	6/7	R	145.5	−9.5	161.5	−49.2	187.6	4.9
Mean[c]					6	R			165.3	−36.4	37.7	11.0
Gongliu area												
527	43.4°N, 82.5°E	Red sandstone	P_2x	93/40	6/8	R	186.5	−17.7	189.5	−59.3	11.0	14.1
528	43.4°N, 82.5°E	Red sandstone	P_2x	93/45	6/8	R	194.9	−6.2	201.6	−49.8	8.7	14.9
529	43.4°N, 82.5°E	Red sandstone	P_2x	95/48	6/7	R	187.5	−14.6	190.3	−62.5	38.7	10.9
530	43.4°N, 82.5°E	Red sandstone	P_2x	92/49	6/8	R	187.7	−25.6	200.9	−73.9	74.3	7.8
531	43.4°N, 82.5°E	Red sandstone	P_2x	100/41	6/9	R	189.4	−16.6	189.4	−57.6	123.4	5.8
Mean					5	R	189.3	−16.2			111.7	7.3
									194.1	−60.7	76.1	8.8
Yuxi area												
549	43.4°N, 84.4°E	Andesite	C_2t	54/15	6/7	R	214.4	−35.7	225.7	−39.3	380.6	3.4
550	43.4°N, 84.4°E	Andesite	C_2t	54/15	6/7	R	212.0	−35.3	223.1	−39.6	411.8	3.3
551	43.4°N, 84.4°E	Andesite	C_2t	54/15	6/7	R	213.0	−37.5	225.1	−41.4	64.7	8.4
552	43.4°N, 84.4°E	Colorful sandstone	C_2t	54/15	6/9	R	207.3	−39.1	220.0	−44.4	60.0	8.7
553	43.4°N, 84.4°E	Andesite	C_2t	54/15	6/7	R	216.9	−32.6	226.9	−35.7	179.2	5.0
554	43.4°N, 84.4°E	Andesite	C_2t	54/15	6/8	R	204.9	−38.0	217.0	−44.0	124.9	4.1
Mean					6	R	211.5	−36.4			354.3	3.6
									223.1	−40.8	350.1	3.6
Axi area												
510	44.2°N, 81.5°E	Grey pelite	O_2l	290/40	9/9	–	–	–	–	–	–	–
511	44.2°N, 81.5°E	Grey pelite	O_2l	260/77	10/10	–	–	–	–	–	–	–
512	44.2°N, 81.5°E	Grey pelite	O_2l	285/78	7/8	–	–	–	–	–	–	–
513	44.2°N, 81.5°E	Grey pelite	O_2l	80/72	7/8	–	–	–	–	–	–	–
514	44.2°N, 81.5°E	Grey pelite	O_2l	255/80	6/7	–	–	–	–	–	–	–
515	44.2°N, 81.5°E	Black limestone	O_2l	320/58	7/7	–	–	–	–	–	–	–

Table 1 (*continued*)

Site	Coordinates	Rocks	Age	Strike/dip	n/N[a]	P	Dg	Ig	Ds	Is	k	α_{95}
Axi area												
516	44.2°N, 81.5°E	Black limestone	O_2l	320/58	8/8	–	–	–	–	–	–	–
517	44.2°N, 81.5°E	Red pelite	O_2l	320/45	6/8	–	–	–	–	–	–	–

Abbreviations: P, polarity; R, reversed; O_{2l}, Ordovician Lelengeledaban Formation (Fm); C_{1ak} and C_{1aw} are Early Carboniferous Akeshake Fm and Awulale Fm; C_{2y} and C_{2t} are Late Carboniferous Yishijilike Fm and Tuergong Fm; P_{2x}, Late Permian Xiaoshansayi Fm; Dg, Ig, Ds, Is are declination (D) and inclination (I) in geographic (g) and stratigraphic (s) coordinates, k is the best estimate of the precision parameter, α_{95} is the radius that mean direction lies within 95% confidence.

[a] n, measured sample number; N, collected sample number.

[b] Ages within the parentheses represent the age of remanence.

[c] Locality-mean direction calculated with 4 in-situ directions of Sites 537–540 and 2 tilt-corrected directions of sites 541 and 542.

experiment, the acquisition of Isothermal Remanent Magnetization (IRM) and the measurements of Anisotropy of Magnetic Susceptibility (AMS) carried out in Laboratoire de Magnétisme des Roches d'Orléans (LMRO), and magnetic hysteretic curves in Laboratoire du Paléomagnétisme of Institut de Physique du Globe de Paris (IPGP) at St Maur.

At least 6 cores were chosen from each site to carry out thermal and/or alternating magnetic field (AF) demagnetization in LMRO and IPGP. About 15 steps have been applied to progressive magnetic remanence cleaning with intervals varying from 20 to 150 °C for thermal and 1 to 20 mT for AF demagnetization.

The magnetic remanent directions were isolated by principal component analysis (Kirschvink, 1980), the mean directions were computed by Fisher (1953) spherical statistics using paleomagnetic software packages offered by Cogné (2003) and PMGSC (version 4.2) by R. Enkin (unpublished).

4. Measurement results

4.1. Zhaosu area

Two Carboniferous formations were sampled: Early Carboniferous Akeshake Formation (C_{1ak}) exposed in the south and Late Carboniferous Yilishijilike Formation (C_{2y}) (XBGMR, 1979a) exposed in the north of the Zhaosu area (Fig. 2b; Table 1).

4.1.1. C_{1ak} Akeshake Formation

Its lithology is composed of red sandstone occasionally bearing andesitic volcanic clasts, and yellow sandstone (Fig. 2b; Table 1). IRM measurement shows an abrupt increase with the total saturation at about 200 mT (Fig. 3a-1 and a-2), indicating predominantly low-coercivity magnetic minerals in rocks. Thermal magnetic measurements display a sharp drop of magnetic susceptibility of sandstone and andesite at around 580 °C (Fig. 4a), showing the existence of titanium-poor magnetite. Two components were isolated from 22 out of 25 measured samples. The low temperature components up to about 150 °C show dispersed directions. Only a reverse polarity has been revealed from the high temperature component isolated from 250–300 to 580 °C, indicating that the magnetic remanence in these rocks is mainly carried by magnetite. Fig. 5b, c and Table 1 present site-mean directions in geographic (g) and stratigraphic (s) coordinates and an age-mean direction was calculated for this locality: Dg=207.3°, Ig=−57.8°, k=10.5, $\alpha_{95\ g}$=29.8° and Ds=180.2°, Is=−40.9°, k=46.9, $\alpha_{95\ s}$=13.6° with n=4 (Table 1). Enkin's (2003) DC fold test gives a positive answer to this formation with the maximum k value at 74.4%±49.7%.

4.1.2. C_{2y} Yilishijilike Formation

Five sites of red sandstones were sampled from a monoclinal section of about 200 m in stratigraphic thickness. IRM and magnetic hysteresis measurements of C_{2y} red sandstone (Figs. 3a-3 and 6a) suggest the occurrence of both low and high coercive magnetic minerals in the rocks. Thermal magnetic experiment also shows an evident drop of magnetic susceptibility from 550–620 °C during the heating process (Fig. 4b) with two blocking temperatures at around 580 °C and 680 °C (Fig. 5d–f), implying the presence of both magnetite and hematite. An age-mean direction has been calculated for this locality: Dg=151.6°, Ig=−61.2°, kg=48.0, $\alpha_{95\ g}$=11.2°, and Ds=164.7°, Is=−47.4°, ks=50.7, $\alpha_{95\ s}$=10.9° with n=5 (Table 1). No fold test could be concluded because of similar bedding, though the precision parameters (k) are improved after tilt-corrections.

4.2. Xinyuan area

Volcanoclastic sandstone and basalt of the Early Carboniferous Awulale Formation (C_{1aw}) (XBGMR, 1975) were collected from 11 sites in the south of Xinyuan County (Fig. 2a). Low-coercivity magnetic

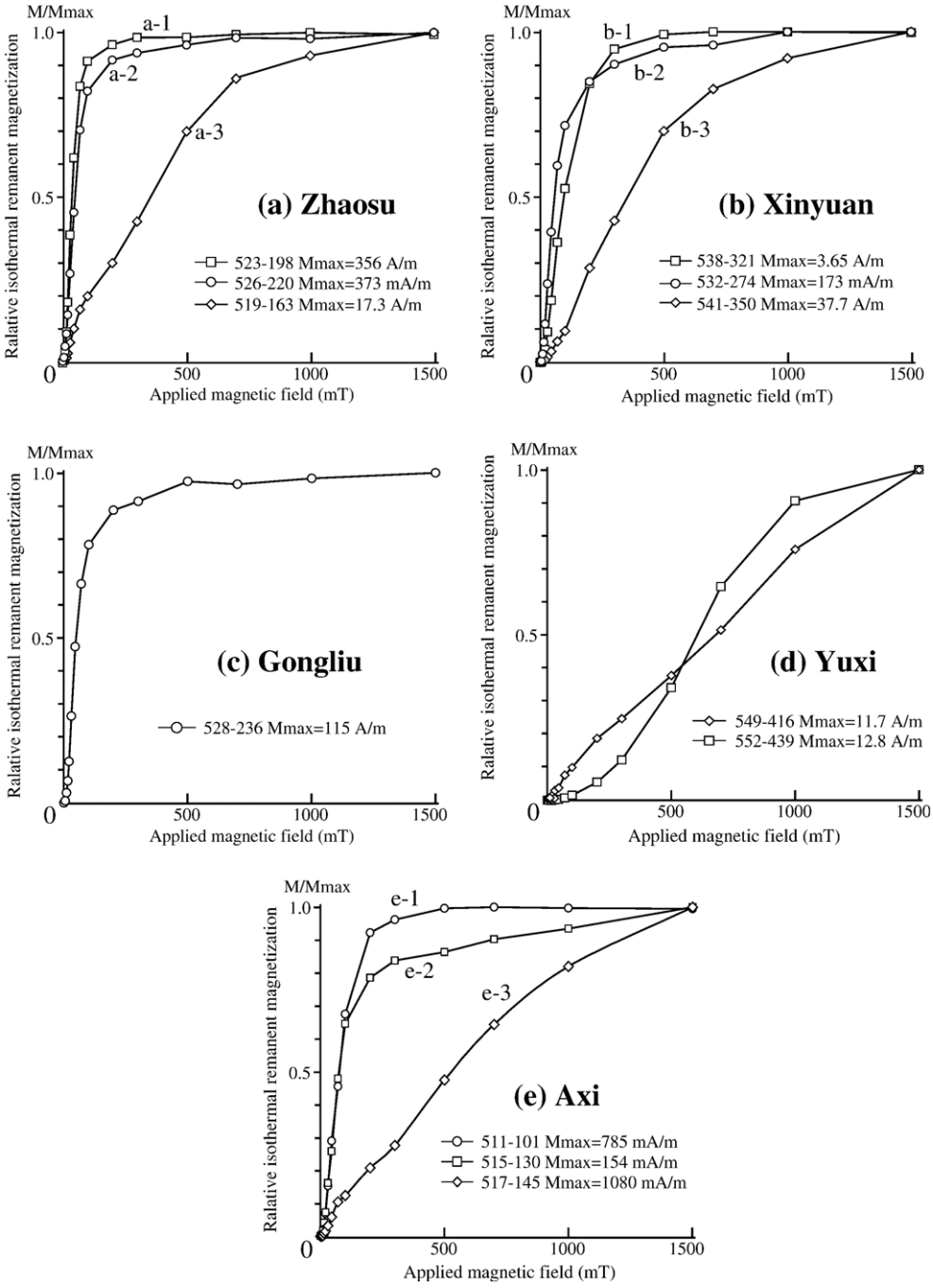

Fig. 3. Isothermal magnetization results of representative cores from each sampled locality.

minerals were identified as the principal remanent carrier for tuffaceous sandstone and basaltic rocks on the basis of (a) abrupt IRM increase with a total magnetic saturation at about 200 mT (Fig. 3b-1 and b-2), (b) Curie temperature point at around 580 °C (Fig. 4c) and (c) narrow wasp-waisted hysteresis loops (Fig. 6b). But mixture of low and high coercivity magnetic minerals in rhyolitic sandstone was meanwhile identified by gradually increasing IRM curve (Fig. 3b-3) and wasp-waisted hysteresis loops (Fig. 6c).

Five sites of tuffaceous sandstone (Sites 532–536, Table 1) show very weak NRM (usually less than 1 mA/m).

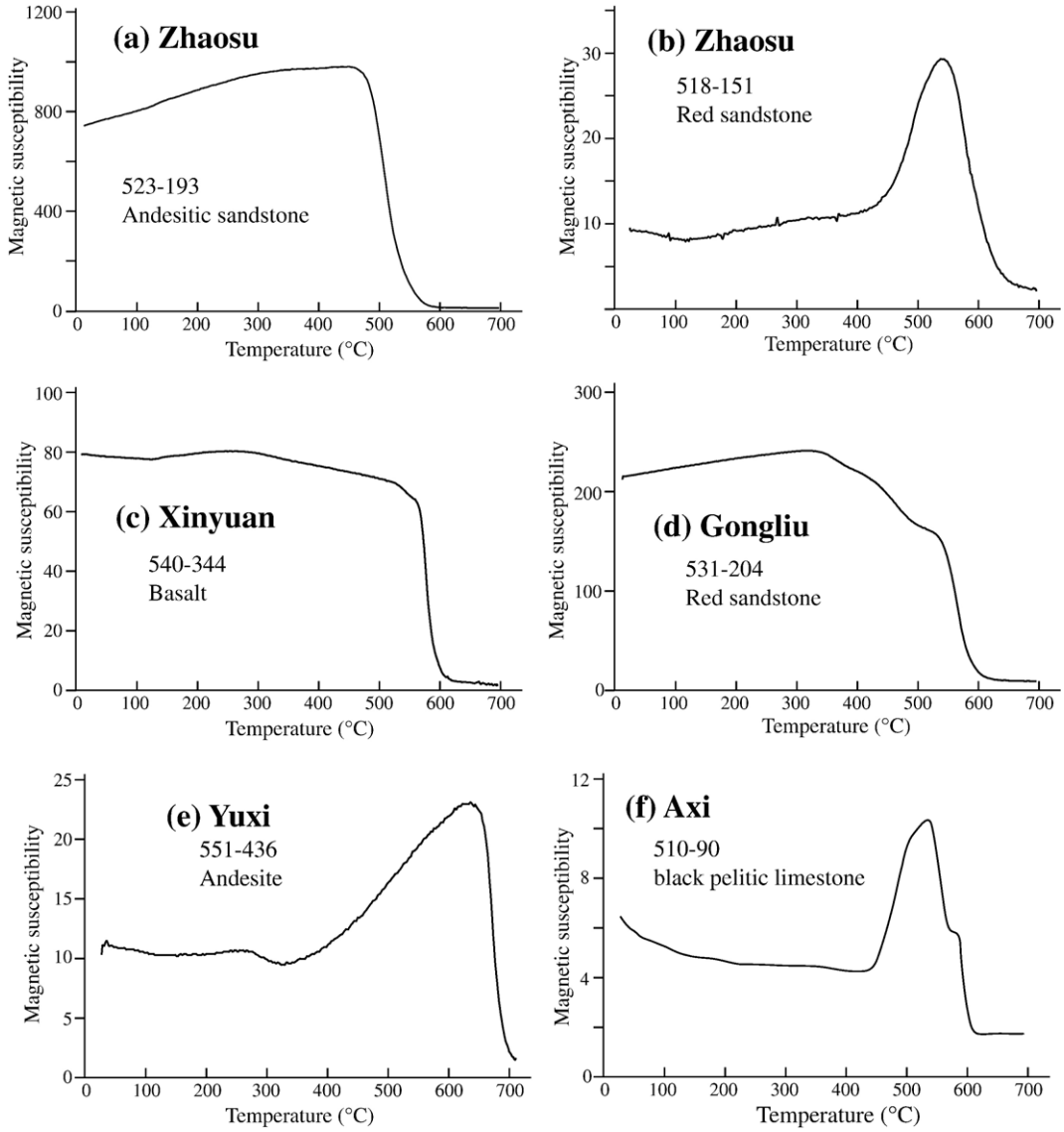

Fig. 4. Results of thermomagnetic Curie temperature analyses on representative lithologies of the Yili Block.

Demagnetization on most of samples displays an important viscous component that may be cleaned up to 350 °C and close to Present Earth Field (PEF; Fig. 7a). After the removal of the magnetic viscosity, most of specimens show random directions due to weak remanent intensity and few specimens show "stable" directions, which are also not far from PEF (Fig. 7b). So, no mean-site directions could be calculated.

Four sites of basalts (Sites 537 to 540, Table 1) show relatively stable and reverse magnetic components isolated at about 90 ~ 110 mT or 580 °C carried mainly by the titanium-poor magnetite (Fig. 7c and d; Table 1). Tilt corrected directions are, however, much less clustered than in-situ directions with a ratio of 0.06 for ks/kg, indicating a negative fold test (Fig. 7e and f).

The remaining 2 sites of red rhyolitic sandstone (Sites 541 and 542) show two blocking temperatures at around 580 °C and 680 °C (Fig. 7g and h), implying the presence of the association of magnetite and hematite. A good consistency may be observed between high temperature components isolated from magnetite and hematite. No fold test may be applied as their bedding is constant. The directions isolated from high temperature component are more consistent in stratigraphic coordinates with those of basalt than in geographic ones (Table 1), a locality-mean has been, therefore, calculated

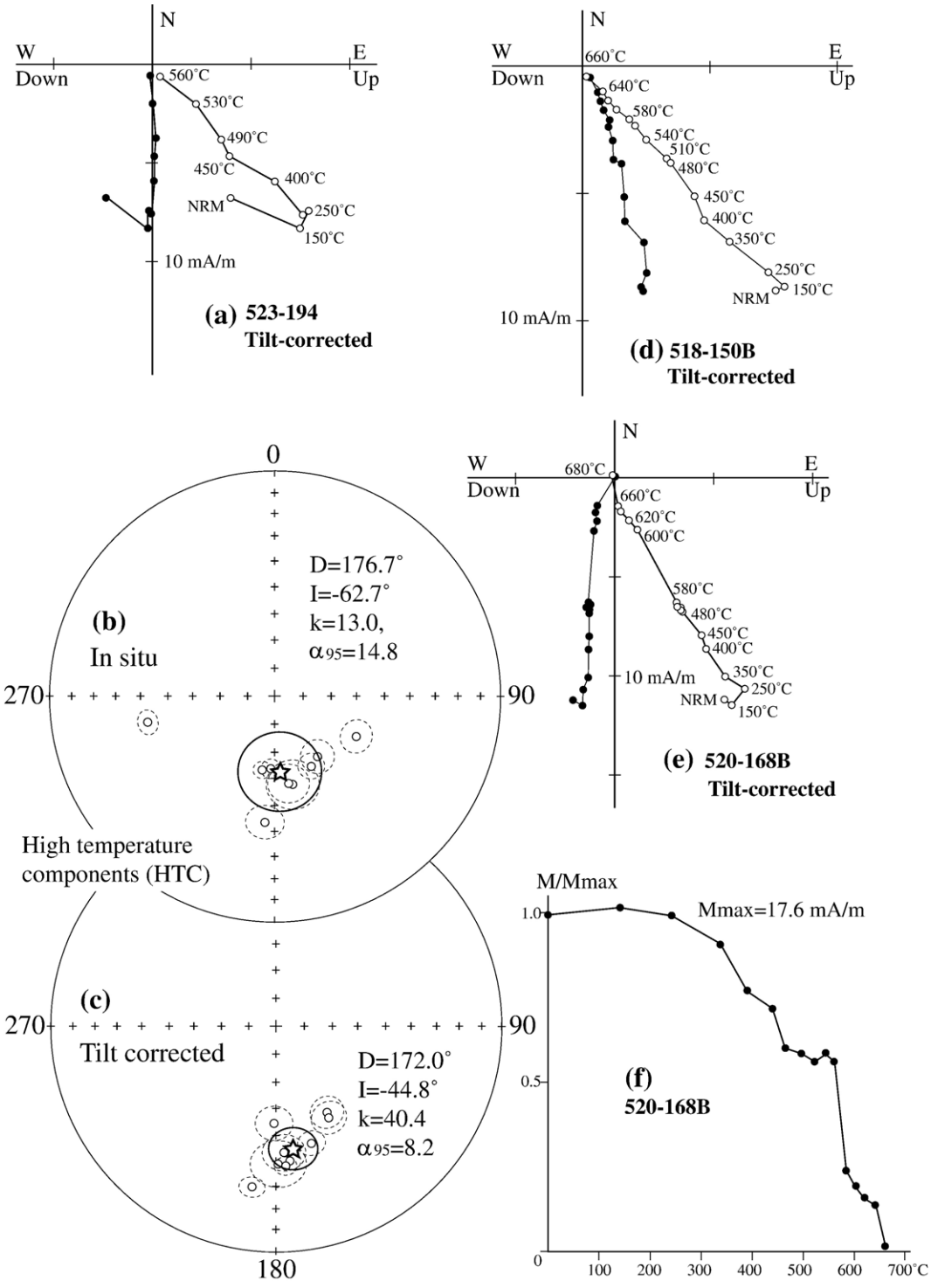

Fig. 5. Measurement results from Zhaosu area. (a–c) Orthogonal projection of sample demagnetization (Zijderveld, 1967) in stratigraphic coordinates and (d) normalized intensity curves of progressive demagnetization. White (black) circles represent vertical (horizontal) plans. (e) and (f) equal-area stereoplots for site-mean directions isolated from high temperature components in geographic and stratigraphic coordinates, respectively. Stars represent the locality-mean directions.

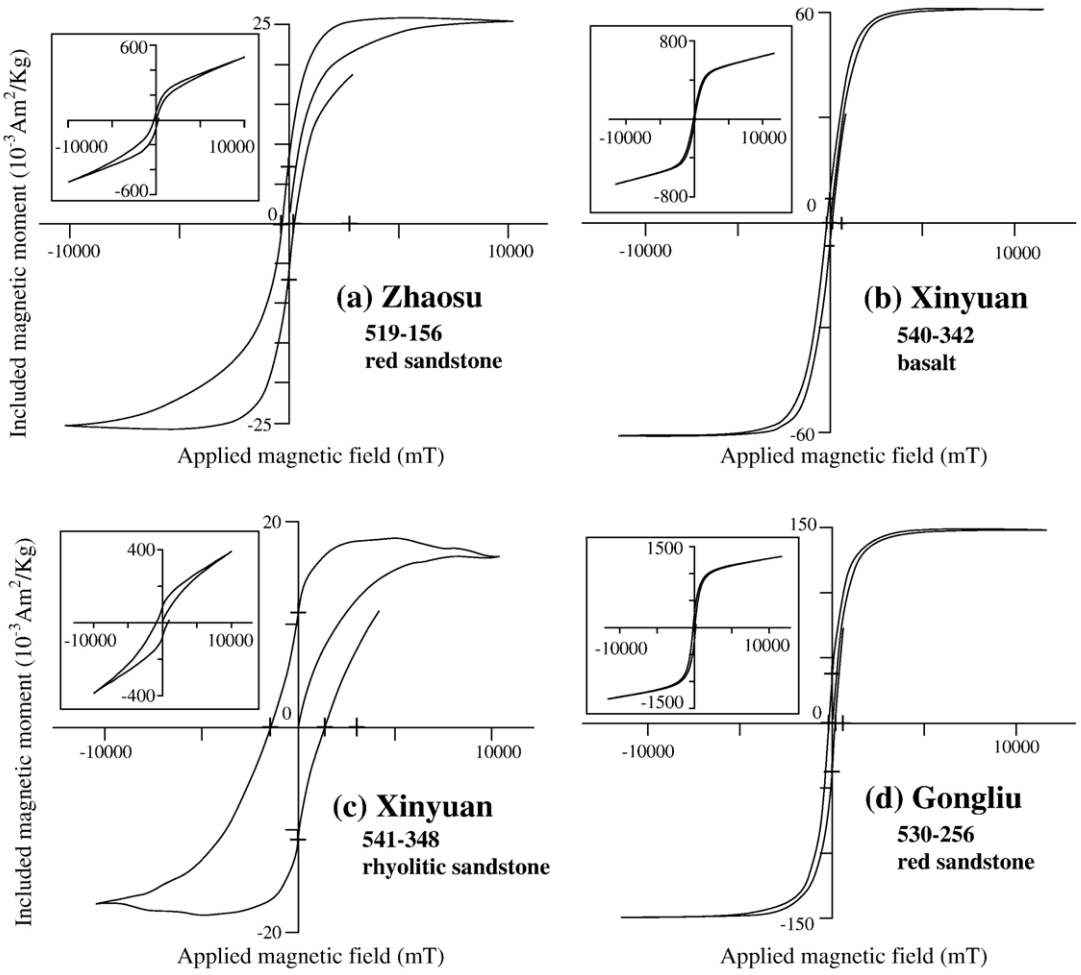

Fig. 6. Representative hysteresis loops of samples from the Yili Block.

from these 2 sites in stratigraphic coordinates with 4 basalt sites in geographic ones (see Discussion for detail explanation; Table 1, Fig. 7e).

4.3. Gongliu area

To the southeast of Gongliu County (Fig. 2a), an excellent exposure of E–W trending Late Permian red beds with a thickness larger than 2000 m is referred to as Xiaoshansayi Formation (P_{2x}) on the basis of plant fossils (XBGMR, 1979b). Titanium-poor magnetite seems to be the main remanent carrier with minor proportion of hematite according to rapid IRM saturation at about 200 mT (Fig. 3c), sharp drop of magnetic susceptibility at Curie point of about 580 °C (Fig. 4d) and typical narrow wasp-waisted magnetite hysteresis (Fig. 6d). The directions carried by both magnetite and hematite are well consistent to each other (Fig. 8a, c and d). All cores display two different remanence components, where the HTC yield a site-mean direction: Dg=189.3°, Ig=−16.2°, kg=111.7, $\alpha_{95\ g}$=7.3° and Ds=194.1°, Is=−60.7°, ks=76.1, $\alpha_{95\ s}$=8.8° with n=5 (Table 1; Fig. 8e and f). The fold test is inconclusive as the variation of bedding is not important enough.

4.4. Yuxi area

Late Carboniferous versicolor sandstones are interbedded with andesite flows near the Yuxi pass (Fig. 2a). Six sites of andesite and sandstone were collected from the Tuergong Formation (C_{2t} XBGMR, 1973, Table 1). Linear or sub-linear IRM curves show characteristic high coercive minerals (Fig. 3d), thermal magnetic experiments identified hematite as the corresponding ones

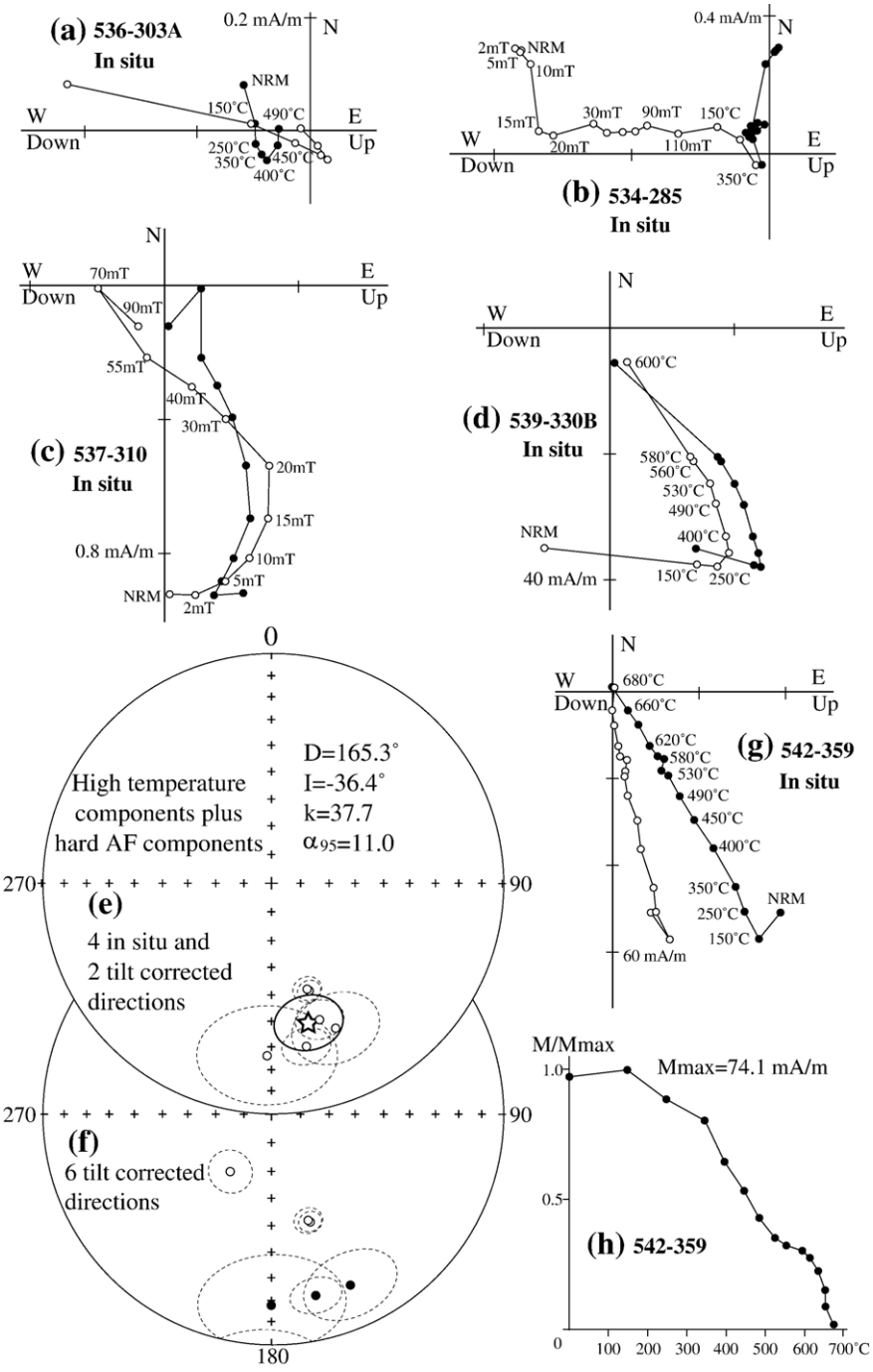

Fig. 7. Measurement results from Xinyuan area. (a–d) and (g) Orthogonal projection in geographic coordinates and (h) normalized intensity curves of progressive demagnetization. (e) and (f) equal-area stereoplots for high temperature and hard AF components. White (black) circles in (e) and (f) represent reversal (normal) polarities of site-mean direction, other symbols are same as in Fig. 5.

(Fig. 4e). Stable high temperature components isolated from magnetic demagnetization yield a mean direction at: Dg=211.5°, Ig=−36.4°, kg=354.3, $\alpha_{95\ g}$=3.6° and Ds=223.1°, Is=−40.8°, ks=350.1, $\alpha_{95\ s}$=3.6° with n=6 (Table 1).

4.5. Axi area

Middle Ordovician pelitic rocks of the Lelengeledaban Formation (O_{2l}) (XBGMR, 1988) were sampled from 8 sites in Axi area (Fig. 2a). Magnetite and hematite are

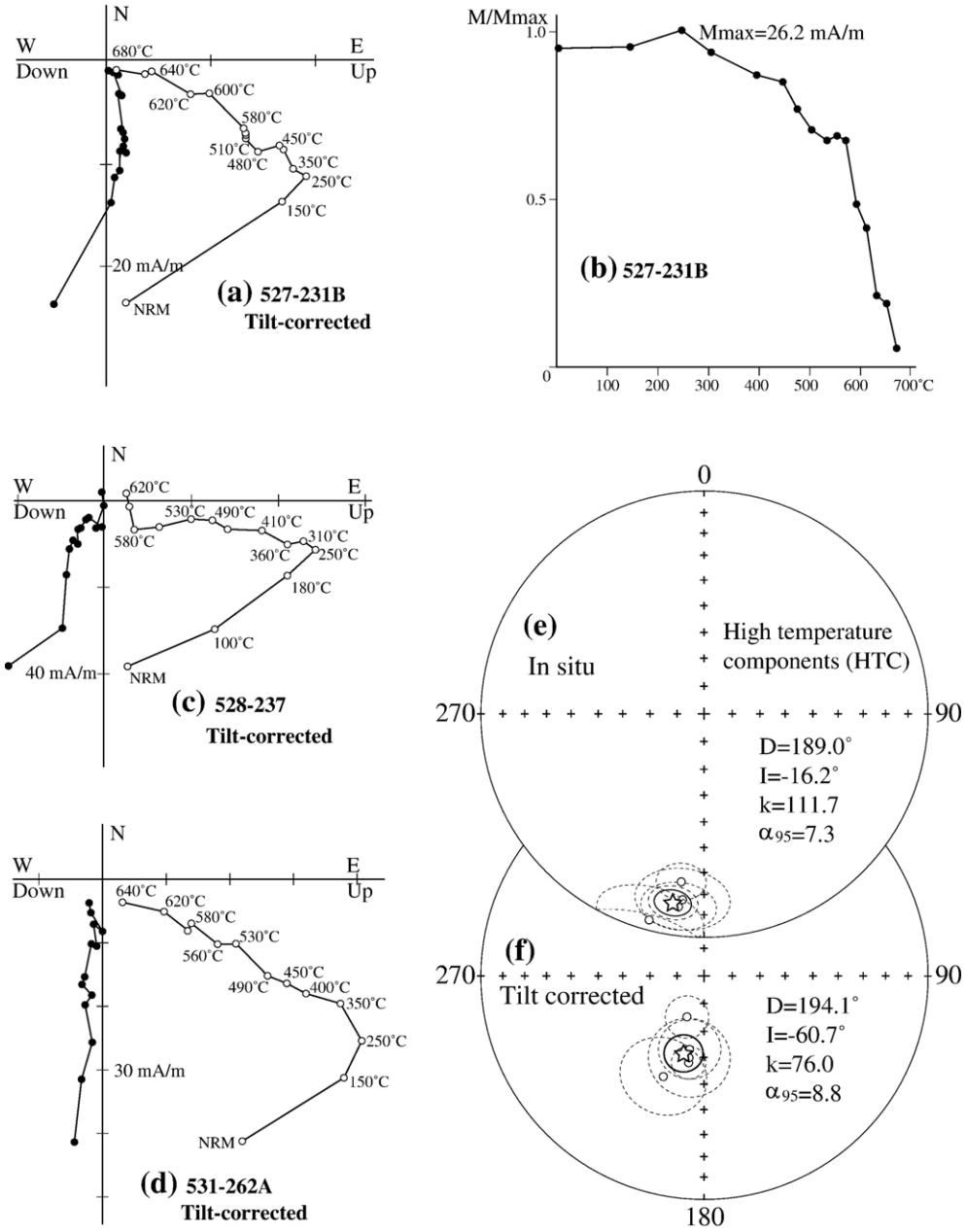

Fig. 8. Measurement results from Gongliu area. (a) and (c–d) Orthogonal projection in stratigraphic coordinates and (b) normalized intensity curves of progressive demagnetization. (e) and (f) equal-area stereoplot for high temperature components in geographic and stratigraphic coordinates, respectively. Symbols are same as in Fig. 5.

suggested to be the main magnetic minerals by IRM studies with a very weak remanent intensity (Fig. 3e). Thermal magnetic experiments show an obvious oxidation and an important proportion of magnetite may be formed during the heating (Fig. 4f). The NRM of pelitic rocks is very heterogeneous and varies from 0.096 to 6.98 mA/m with an average of 0.25 mA/m. No any stable component may be isolated after the removal of viscous magnetization.

5. Discussion

Except for the samples from the Axi section that yield no reliable magnetic component, laboratory magnetic

mineralogical analyses and thermal/AF demagnetizations have successfully isolated two magnetic components, namely viscous and characteristic remanent magnetizations from 4 out of 5 Late Paleozoic sections. The viscous one clearly records the recent geomagnetic field with a negative fold test (Dg=348.4°, Ig=67.1°, kg=15.9, $\alpha_{95\ g}$=3.1° and Ds=350.2°, Is=52.9°, ks=3.3, $\alpha_{95\ s}$=7.9° with n=185 samples). However, the stable titanium-poor magnetite and hematite have been identified as principal magnetic remanent carriers for the characteristic remanent magnetization. The following evidences strengthen our argument that the ChrM can be used for tectonic implications: (1) the positive fold test observed from Zhaosu area; (2) the solo reversed polarity with significantly distinguishable mean directions from PEF as well other Mesozoic and Cenozoic ones (Chen et al., 1992, 1993). However, as mentioned above, this area has experienced multi-phase tectonic and magmatic events. Before putting forward their tectonic implications of these new paleomagnetic data, their reliability and magnetic remanence age should be discussed.

5.1. Reliability and magnetic remanence age

In order to acknowledge on the degree of deformation for our paleomagnetic collection, Anisotropy of Magnetic Susceptibility (AMS) measurements were performed. Fig. 9 reveals a relatively weak anisotropy degree with $P'<1.05$ for most of samples though some from Yuxi and Axi seem to have higher and heterogeneous P' values. This observation indicates that the sampling zones have not suffered severe latter deformation at least at the hand-sample scale.

Table 1 shows rock ages of our collection ranging from Early Carboniferous to Late Permian. The exclusive reversal polarity revealed from ChrM seems consistent with the Permo-Carboniferous Reversed Superchron (PCRS), e.g. by Hounslow et al. (2004). However, as described in the Geological Setting section, some Late Carboniferous volcanic rocks overlie the Lower Carboniferous sedimentary rocks and, the folding is younger than the volcanism. Furthermore, Carboniferous–Permian granitic plutons are often found near the sampling sites, thus we cannot simply conclude that the remanence isolated from ChrM is primary nor calculate age-mean directions and corresponding paleomagnetic poles.

For the Late Permian rocks of Gongliu area, their age is well constrained by abundant plant fossils and they are unconformably overlain well-dated Early Permian volcanic rocks. Though the statistic precision parameter (k) slightly decreases, the fold test is not conclusive due to weak bedding variation. Thus, the solo reversed polarity from about 300 m-thick section may indicate that the magnetic remanence has been acquired before ~250 Ma (the upper limit of PCRS), i.e. similar to the Late Permian rock age. Thus, a paleomagnetic pole has been calculated for P_2 period: λ=79.7°N, ϕ=172.0°E, A_{95}=11.3° with n=5 (Table 2).

Four sites from the Early Carboniferous Akeshake formation (C_{1ak}) show also only one reversed polarity with a positive fold test. If the paleomagnetic collection was representative for this geological period, the normal polarity should be identified by demagnetization since the C_1 and C_2 limit is close to the lower limit of PCRS (~325 Ma). Geologically, Early Permian intra-continental volcaniclastic rocks (XBGMR, 1993; Allen et al.,

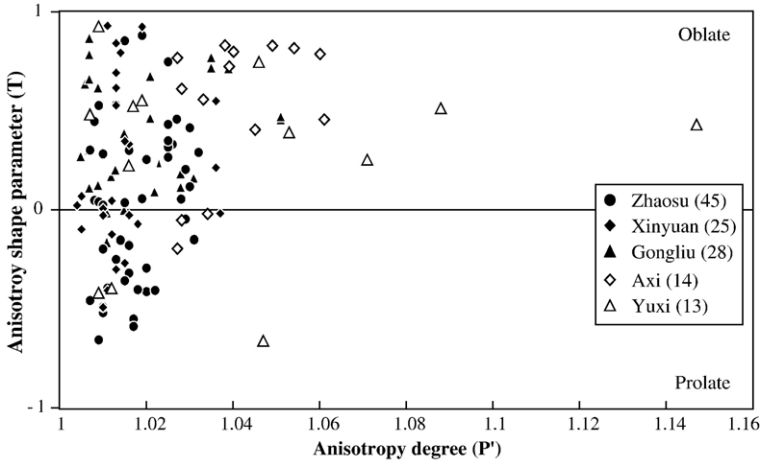

Fig. 9. Plots of anisotropy degree (P') versus anisotropy shape (T) of magnetic susceptibility for volcanic and sedimentary rocks in the Yili Block and its adjacent areas. $P'=\exp\{2[(\ln K1-\ln Km)^2+(\ln K2-\ln Km)^2+(\ln K3-\ln Km)^2]^{1/2}\}$, and $T=2\ln(K2/K3)/\ln(K1/K3)-1$, where $K1$, $K2$ and $K3$ are principal axes of the magnetic fabrics and Km is their average.

Table 2
Synthesis of Late Carboniferous and Late Permian paleomagnetic poles from the Yili, Junggar, Tarim and Siberia blocks

Blocks	Areas	Ages	Slat	Slong	N	Plat	Plong	A_{95}	References
Yili	Gongliu	P_2	43.4	82.5	5	79.7	172.0	11.3	This study
	Zhaosu	C_2	43.3	81.1	9	72.0	287.1	8.9	This study
	Xinyuan	C_2	43.3	83.3	6	63.9	296.0	9.8	This study
	Mean	C_2			15	68.6	290.6	6.1	This study
Tarim	Northwest	P_2	40.2	79	21	65.6	181.2	3.9	Li et al. (1989)
	Southwest	P	37	80	8	65.4	170.5	8.5	Gilder et al. (1996)
		P2	40.8	79.8	24	62.9	190.7	6.3	Gilder et al. (1996)
		P2			20	66.0	188.8	6.3	Meng (1991)
		P2	42.1	83.4	10	73.2	191.0	7.3	Li et al. (1991)
	Mean	P_2				66.8	184.1	4.9	
	Southwest	C_2	37	80	7	60.2	165.4	11.1	Gilder et al. (1996)
	Akesu	C_2	40.3	79.5	44	52.2	179.5	8.6	Van Der Voo (1993)
	Akesu	C_2	40.6	79.5	9	46.5	168.0	4.6	Zhao et al. (2003)
		C_2	40.5	78.8	3	41.0	160.0	4.0	Sharps et al. (1992)
		C_2			44	61.3	174.0	4.0	Nie et al. (1993)
		C_2			22	46.6	170.2	4.5	Harkand et al. (2005)
	Mean	C_2				51.5	169.1	7.7	
Siberia		P_2			5	50.0	160.0	7.0	Van Der Voo (1993)
		C_2			17	41.0	169.0	3.0	Van Der Voo (1993)
Junggar	Tianchi	P_2	44	88.1	7	76.0	193.0	4.6	Nie et al. (1993)
	Urumqi [a]	P_2	43.8	87.7	78 [b]	77.7	0.4	5.5	Sharps et al. (1992)
	Northwest [c]	C_2–P	47.2	86.6	26	69.0	350.0	7.5	Li et al. (1991)
	Northwest [c]	C_2–P	45.6	83.2	23	78.0	238.7	7.9	Li et al. (1989)
	Urumqi [c]	C_2–P	43.8	87.8	4	69.0	231.0	13.7	Li et al. (1991)
	Urumqi [c]	C_2–P	43.8	87.8	7	55.0	172.0	15.1	Li et al. (1991)
	Northwest	C_2	46.7	86.1	15	70.0	299.0	6.4	Li et al. (1991)

Abbreviations: Slat (Plat) is the latitude of site (pole), Slong (Plong) is the longitude of site (pole); α_{95} is the radius that mean direction lies within 95% confidence, N is the number of sites.
[a] Viscous, only 26 out of 78 samples give directly observed directions of 4 sites, and these directions are dispersed. Others are analysed with grand circle.
[b] Sample number.
[c] Ages are uncertain; and directions are explained with considerable later overprint.

1995; Shu et al., 2005) overlay unconformably on the folded Late Carboniferous volcano-sedimentary rocks in the Yili Block, indicating that folding occurred before Early Permian magmatism. Moreover, the site-mean directions of the Early Carboniferous are very close to those of the Late Carboniferous, and both of them are obviously different from the direction of the Late Permian red beds (Table 1). This unconformity and positive fold test exclude the possibility of an Early Permian overprint. Additionally, since both C_1 and C_2 sandstones are covered by homochronous volcanic rocks and intruded by granites, which are dated by zircon U–Pb from 361±6 Ma to 309±3 Ma (Zhu et al., 2005; Wang et al., 2006), suggesting that the thermal event corresponding to the Yili magmatic arc lasted until the end of Late Carboniferous. This prominent thermal event might be responsible for re-magnetization of the pre-existing rocks. It is, therefore, reasonable to suggest that both Early and Late Carboniferous rocks of Zhaosu area recorded an identical paleomagnetic direction during the Late Carboniferous magmatism in the Yili Block. Thus, an overall mean direction is calculated for both Early and Late Carboniferous sites: Dg=176.7°, Ig=−62.7°, kg=13.0, $\alpha_{95\ g}$=14.7° and Ds=172.0°, Is=−44.8°, ks=40.4, $\alpha_{95\ s}$=8.2° (Table 1; Fig. 5b–c).

A similar situation occurs for the Early Carboniferous rocks from Xinyuan area. All reliable directions of basalts from Sites 537–540 show a reversed polarity in geographic coordinate but with a negative fold test (Table 1; Fig. 7e and f), indicating latter overprint instead of primary magnetization for these Early Carboniferous samples. Due to the high occurrence of volcanic rocks dated at 313±4 Ma (Zhu et al., 2005) and granites at 315±3 and 309±3 Ma in the sampling area (Wang et al., 2006) (Fig. 2a), it is reasonable to propose a Late Carboniferous (~310 Ma) age for the thermal re-magnetization. Concerning the two rhyolitic sandstone sites (Sites 541–542), although the reversal polarity is identified in both coordinates, their directions in stratigraphic coordinates seem more consistent with either the in-situ directions of 4 volcanic sites or the locality-mean direction of Zhaosu area. The age of the rhyolitic sandstone is, in fact,

questionable. No any direct age constraint has been documented from this formation although referred to as Early Carboniferous (XBGMR, 1993; XBGMR, 1975). In the point of view of regional tectonics and stratigraphic correlation, it is clear that the age of the rhyolitic sandstone is younger than that of the basalt dated at 354±5 Ma (zircon U–Pb SHRIMP by Zhu et al., 2005). Moreover, no any direct contact between these two lithostratigraphic units can be observed in the field, stratigraphic and structural knowledge allows us to exclude a syncline structure and to favour an unconformable contact. According to the above arguments, it is not unreasonable to consider that the rhyolitic sandstone is Late Carboniferous in age. Thus, 4 in-situ paleomagnetic directions of basalts and 2 tilt-corrected directions of rhyolitic sandstones are used to calculate an average direction at: D=165.3°, I=−36.4°, k=37.7, α_{95}=11.0° for the Late Carboniferous magnetization from Xinyuan area (Table 1; Fig. 7e).

As to paleomagnetic results from Yuxi area, 6 Late Carboniferous sites present well-grouped reversal directions without fold test due to monoclinal attitude of the bedding (Table 1). The magnetic inclinations from this locality are consistent with those from Zhaosu and Xinyuan areas, but this area shows a significant different declination with respect to the other two. As this sampling locality is situated close to a tectonic zone (Fig. 2a), the difference in declination may be explained by a local rotation of the Yuxi sampling zone with respect to the Yili Block.

According to above direction analyses and geologic arguments, a C_2 paleomagnetic pole may be calculated for the Yili Block from Zhaosu and Xinyuan areas: λ=68.6°N, ϕ=290.6°E, A_{95}=6.1° with n=15 (Table 2).

5.2. Comparisons of the paleomagnetic data from Yili with other adjacent blocks

Up to now, no paleomagnetic data were documented from the Yili Block, except some data obtained from Carboniferous–Permian rocks in the western Tianshan of Kyrgyzstan (Bazhenov et al., 1993, 1999, 2003). Most of these data were derived from the deformation belt, e.g. “North Tianshan tectonic zone” located in the extremely northwestern part of the Tianshan Belt (Fig. 1a). These studied areas cannot be considered as a part of a rigid block, some deflections of declination with respect to the reference blocks (e.g. Tarim and Siberia) may be, therefore, interpreted as the result of strike–slip faulting within the orogenic belt, rather than the representative rotation of a rigid body (Bazhenov et al., 1999). In fact, the Yili Block is accepted as a microcontinent with a Precambrian basement (Allen et al., 1992; Gao et al., 1998; Chen et al., 1999; Wang et al., 2006, 2007), it extends westwards into Kazakhstan with an unclear boundary, and its eastern boundaries are the southern and northern branches of the Tianshan range (Fig. 1). These boundaries were highly deformed during the Tianshan orogeny, but the interior of the block is much less deformed. This agrees well with the good consistency between the C_2 paleomagnetic results from Zhaosu and Xinyuan areas located near to the center of the Yili Block but distant from about 200 km (Figs. 2a, 5f and 7e). Thus, the paleomagnetic poles derived from these areas are representative for the whole Yili block (Table 2).

In order to understand the kinematic relationships during the Late Paleozoic between the Yili Block and adjacent ones, previous paleomagnetic results on the Tarim, Junggar and Siberia blocks are analysed and listed in Table 2. Late Carboniferous and Late Permian poles of the Tarim Block have been well documented by numerous studies (Cheng et al., 1983; Bai et al., 1987; Li et al., 1988; McFadden et al., 1988; Zhai et al., 1988; Fang et al., 1990, 1996; Meng and Zheng, 1990; Meng, 1991; Gilder et al., 1996), these data are very consistent with each other within the relatively weak uncertainty (Table 2), the Late Carboniferous and Late Permian mean poles are recalculated at 51.5°N, 169.1°E, A_{95}=7.7° and 66.8°N, 184.1°E, A_{95}=4.9, respectively. Van der Voo (1993) presented Late Carboniferous and Late Permian paleomagnetic poles of Siberia Block (Table 2). As for the Junggar Block, few results have been reported from the Urumqi area and the northwestern Junggar basin (Fig. 1b; Li et al., 1989, 1991; Sharps et al., 1992; Nie et al., 1993), but the available data are quite dispersed, and the ages of magnetization are often undetermined (Table 2). For example, the paleomagnetic results from the southern and northwestern parts of the Junggar basin by Li et al. (1991) are not consistent, an important second overprint is proposed, the ages of the primary or secondary magnetization are roughly restricted between Late Carboniferous and Permian, i.e. a long and variable interval from 20 to 75 Ma. Such an uncertainty in age and variability in paleomagnetic pole make them unfeasible to compare with those from other blocks. Only one relatively reliable paleomagnetic pole derived from the northwestern part of the Junggar basin (Li et al., 1991) may be considered for the Late Carboniferous period (Table 2). Concerning the Late Permian period, two paleomagnetic poles have been obtained from Urumqi (Sharps et al., 1992) and Tianchi areas (Nie et al., 1993) (Table 2). However, the former study shows that only 26 (4 sites) out of 78 samples from Urumqi display directly observable directions, and the other samples are analysed by the grand circle technique with an important uncertainty. In addition, magnetic remanence of these

Late Permian sediments is viscous, magnetic directions are relatively dispersed within and among sites, the paleomagnetic pole is calculated with specimens instead of by site-mean directions. Paleomagnetic directions derived from the Tianchi section seem to be relatively stable, and passed a positive fold test, therefore, these latter results are accepted for the Late Permian paleomagnetic pole of the Junggar block (Table 2).

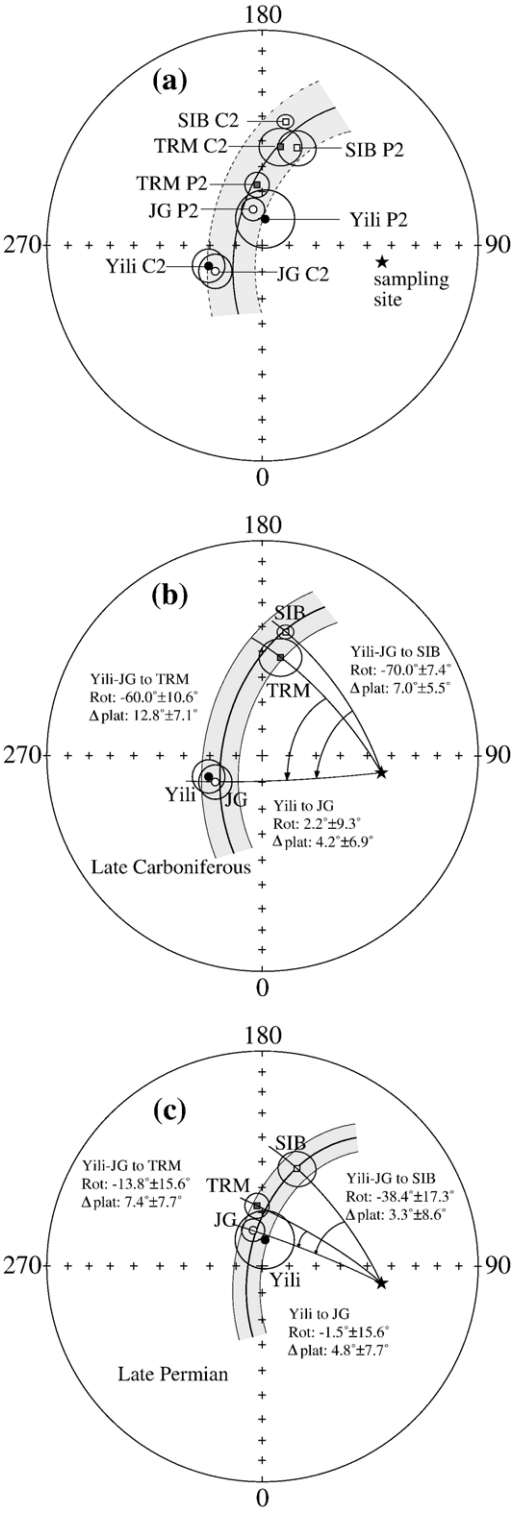

Fig. 10a shows the paleomagnetic poles of each block for each geologic epoch. The Late Carboniferous pole of the Yili Block is very close to that of Junggar with an angular difference of 7.7°±6.6°, but far away from coeval poles of Tarim (120.5°±7.0°) and Siberia (119.0°±5.1°; Fig. 10b). Small circles centred at the sampling site show no significant latitudinal differences of 4.2°±6.9° between Yili Block and Junggar, and relatively weak latitudinal differences of 12.8°±7.1° between Yili and Tarim, and of 7.0°±5.5° between Yili and Siberia (Fig. 10b). The case will be changed when looking at relative rotations. The Yili Block doesn't show any significant relative rotation with respect to Junggar (2.2°±9.3°), but significant counterclockwise (CCW) rotations of 60.0°±10.6° and 70.0°±7.4° with respect to Tarim and Siberia, respectively (Fig. 10b). The Late Permian poles of Yili Block, Junggar and Tarim become almost consistent within uncertainty (<12.1°±9.9°), but they are significantly different from the pole of Siberia (>24.1°±6.8°; Fig. 10c). Latitudinal differences of the Yili Block become insignificant of 4.8°±7.7°, 7.4°±7.7° and 3.3°±8.6° with respect to Junggar, Tarim and Siberia, respectively (Fig. 10c). The CCW rotation of the Yili Block keeps the same of 1.5°±15.6° with Junggar, becomes insignificant of 13.8°±15.6° with Tarim and remains still important of 38.4°±17.3° with Siberia (Fig. 10c).

5.3. Tectonic implications

According to the above presented paleomagnetic data analyses, the observed small latitudinal differences of the Yili Block with respect to Junggar, Tarim and Siberia are within the error bars. This result indicates that no important relative latitudinal movement between the

Fig. 10. (a) Equal-area projections of Late Carboniferous and Late Permian poles of Yili Block, Tarim (TRM), Junggar (JG) and Siberia (SIB), showing that little or no relative latitudinal movement among these blocks, (b) small circle passing through Late Carboniferous poles and grand circles from sampling site to each pole showing significant longitudinal differences between different blocks, (c) no significant longitudinal differences between Yili, Junggar and Tarim shown by small circles passing through Late Permian pole, but a significant longitudinal difference exited between Siberia and the other blocks at Late Permian time. Rot and Δplat stand for relative rotation and convergence with corresponding uncertainties. The positive mean value stands for clockwise rotation and latitudinal shortening, respectively.

Yili Block and the other Central Asia blocks took place since the Late Carboniferous. This observation is quite consistent with geological evidences, from which the major orogenic event in the Chinese Tianshan Belt that is due to the convergences among Junggar, Yili Block and Tarim is considered to have been completed at the end of the Late Carboniferous (Windley et al., 1990; Allen et al., 1992; Gao et al., 1998; Wang et al., 2006). The remaining small convergent latitudinal differences of the Yili Block relative to the other blocks since Late Permian likely correspond to the Cenozoic intra-continental subduction of Tarim and Junggar beneath the Tianshan Belt, and consequent N–S crustal shortening (Tapponnier and Molnar, 1979; Chen et al., 1992; Avouac et al., 1993; Burchfiel et al., 1999; Charreau et al., 2005; Shu et al., 2005).

The good consistency between the paleomagnetic poles from the Yili Block and Junggar may indicate that these two blocks were welded since the Late Carboniferous and they might be paleomagnetically considered as a single block from then on. In another words, if there is any relative motion between them, it should be under the paleomagnetic uncertainty. As described above, the significant polar differences of the Yili Block with respect to Tarim and Siberia essentially reveal the CCW rotations of Yili–Junggar related to Tarim and Siberia. These CCW rotations are estimated of 60.0°±10.6° and 70.0°±7.4° since the C_2 period, and of 13.8°±15.6° and 38.4°±17.3° since the P_2 period (Fig. 10). These observations allow us to estimate the relative rotation from Late Carboniferous to Late Permian by subtracting the relative motion since P_2 from that since C_2. Consequently, during the C_2–P_2 interval, the CCW rotation of the Yili–Junggar Block attained about 46.2°±15.1° with respect to Tarim, and 31.6°±15.1° relative to Siberia. Since Late Permian, this CCW rotation of Yili–Junggar Block with respect to Tarim becomes insignificant within uncertainty (13.8°±15.6°), but remains still significant of 38.4°±17.3° with respect to Siberia. As all four blocks were amalgamated at the end of Late Carboniferous, the relative rotations between blocks were accommodated by strike–slip faulting along their boundaries and therefore resulted in lateral displacements. The northern and southern boundaries of the Yili Block correspond to two ductile shear zones (Fig. 1b). To the north, the North Tianshan Fault (NTF) (Zhou et al., 2001; Zhao et al., 2003; Wang et al., 2006) extends eastward merging in the Main Tianshan Shear Zone (MTSZ) (Laurent-Charvet et al., 2002, 2003). The kinematics of the ductile shearing along the MTSZ and NTF is dextral (Laurent-Charvet et al., 2002, 2003; Wang et al., 2006) (Figs. 1b, 2a and 11a). To the south, the Nalati Fault (NF) (Zhao et al., 2003) and Qingbulak Fault (QF) (Windley et al., 1990; Allen et al., 1992) extend sub-parallelly to the NTF and MTSZ. The Nalati Fault, also regarded as the Nikolaev Tectonic Line (Burtman, 1975), is the most significant structure. Previous studies

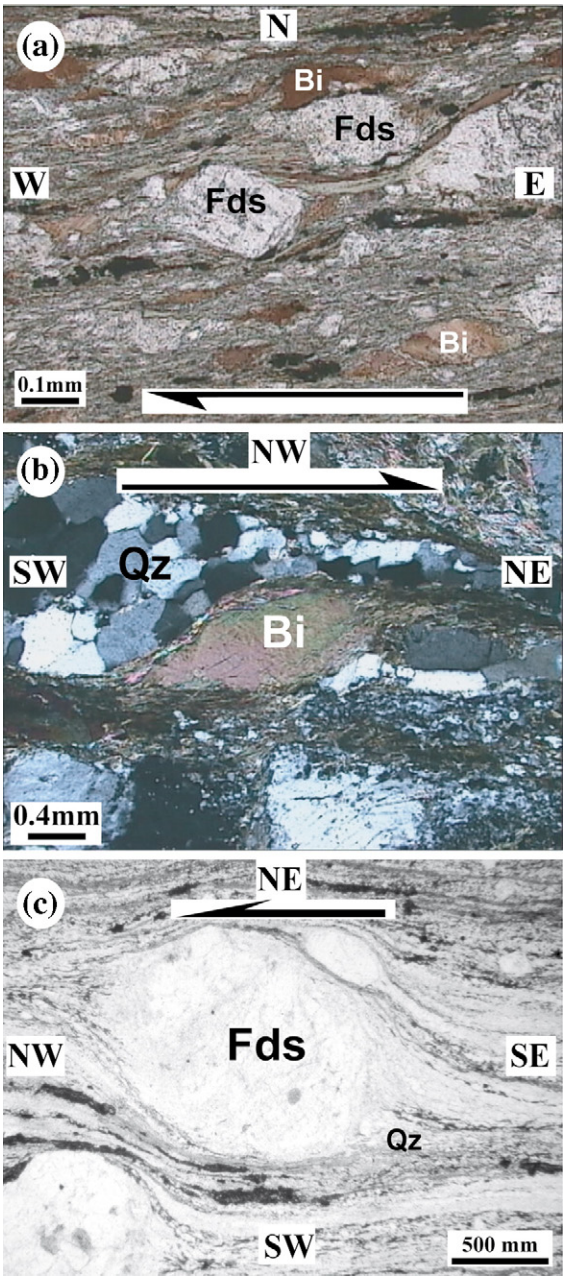

Fig. 11. Microscopic kinematic indicators from ductile strike–slip shear zones, (a) feldspar clasts with biotite pressure shadow showing dextral signature of the North Tianshan shear zone; (b) mica-fish and oblique quartz sub-grain textures indicating dextral shearing along the Nalati Fault; (c) sigmoidal feldspar clast with pressure shadows of quartz and biotite showing sinistral movement of the Erqishi shear zone in the Altay Belt.

proposed a left-lateral slip (Sengör et al., 1993; Allen et al., 1995; Bazhenov et al., 1999), but field structural analyses based on kinematic indicators suggest a right-lateral strike–slip faulting (Yin and Nie, 1996; Wang et al., in review) (Fig. 11b). In order to account for the paleomagnetic and structural data, simplified paleogeographic reconstructions of these rotation patterns are proposed in Fig. 12a, b and c at C_2, P_2 and Present periods, respectively. The quantitative estimation of the lateral displacements corresponding to the CCW rotation of Yili–Junggar with respect to Tarim, requires the definition of a Euler pole of relative motion, around which, one crustal block rotates with respect to another along a major fault. In the Tianshan Range, two strike–slip shear zones form an arcuate belt separating Junggar to the north from Tarim to the south (Fig. 12c). The best fitting small circle passing through this belt allows us to estimate the Euler pole position at about 55°N, 92°E with a radius of about 13° (distance between the pole and the belt; Fig. 12c). The 46.2°±15.1° CCW rotation of Junggar–Yili with respect to Tarim, therefore, corresponds to a right-lateral displacement of 1160±380 km along these strike–slip faults (Fig. 12a and b). This sum of motion may be explained by two opposite displacements of Yili–Junggar and Tarim along the Tianshan shearing zones from C_2 to P_2. During this period, Yili–Junggar experienced an eastward movement of 670±320 km, and Tarim went westwards of 360±270 km, with respect to Siberia, respectively (Fig. 12a and b). It is worth to note that the Central Tianshan located between the Yili Block and Tarim is not involved in our simplified reconstruction.

Similarly, the CCW rotation of Yili–Junggar relative to Siberia was accommodated by a sinistral shearing along the Erqishi ductile shear zone in the Altay Belt (Figs. 1b, 12a, b and c). A sinistral kinematics has been widely recognized by structural analyses (Allen et al., 1995; Shu et al., 1999; Laurent-Charvet et al., 2002, 2003) (Fig. 11c). On the basis of the curved shape of the shear zone (Fig. 12), a Euler pole is estimated at 56°N, 101°E with a radius of about 11° (Fig. 12c). The 31.6°±15.1° CCW rotation of Junggar–Yili with respect to Siberia observed in this study corresponds to a displacement of 670±320 km along the Erqishi Fault during Late Carboniferous to Late Permian (Fig. 12b), and the remaining 38.4°±17.3° CCW rotation implies a continuous displacement of 820±370 km that occurred in post-Permian time (Fig. 12b). It may indicate that Yili–Junggar continued its eastward movement together with Tarim after the

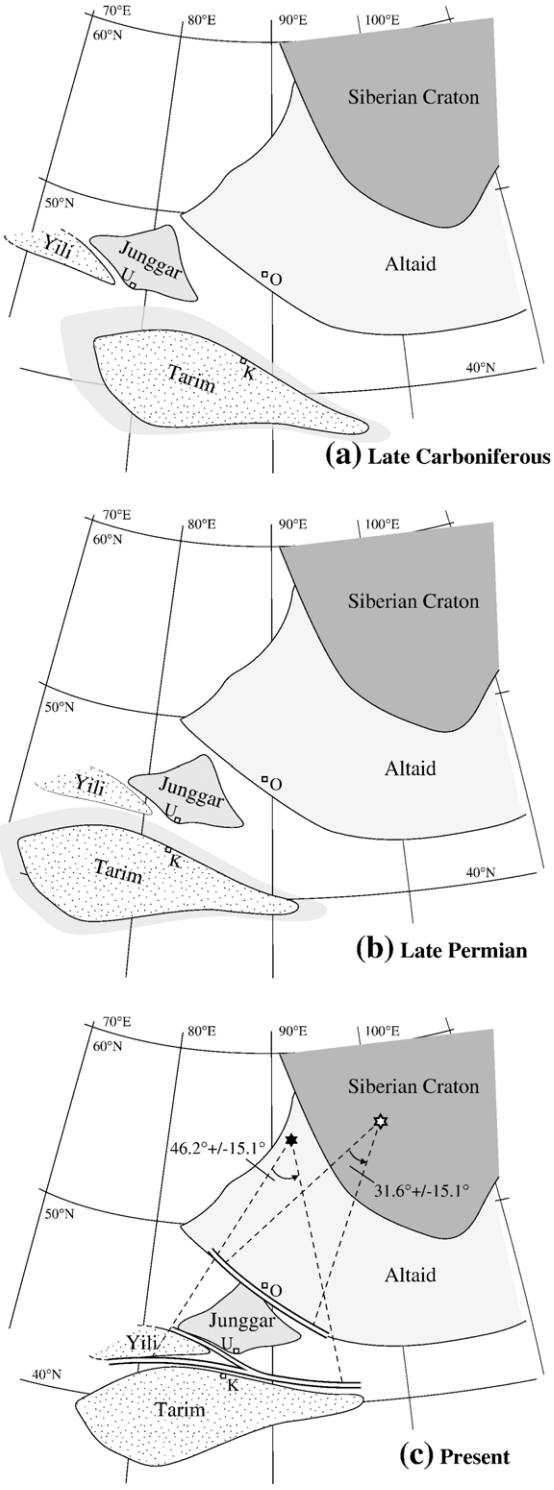

Fig. 12. Simplified reconstruction maps showing the relative rotations of major blocks and consequent lateral displacements along their boundaries by fixing Siberia at its present position. Late Carboniferous (a), Late Permian (b) and Present (c) states are compared. Shadowed zones around the Tarim indicate the subducted margins of Tarim during Cenozoic intra-continental deformation. K, U and O stand for Korla, Urumqi and Ölgij (Mongolian).

Permian (Fig. 12b and c). This motion essentially ended up before the Cretaceous because Cretaceous paleomagnetic data from Junggar, Mongolia as well as Siberia do not show significant differences among them (Chen et al., 1993; Harkand et al., 2005).

Ar–Ar geochronological studies on the ductile deformed rocks from shear zones indicate that Tianshan dextral strike–slip faulting took place during 290 ~ 240 Ma (Yin and Nie, 1996; Zhou et al., 2001; Laurent-Charvet et al., 2002, 2003). Erqishi sinistral strike–slip faulting was also proposed to occur from 290 Ma to 240 Ma (Laurent-Charvet et al., 2003), and continued through Triassic to Early Jurassic (Allen et al., 1995). Such large-scale and contemporaneous displacements along the southern right-lateral and northern left-lateral boundaries of Yili–Junggar blocks enable us to suggest an eastward wedging of Yili–Junggar blocks between Tarim and Siberia. Meanwhile, further paleomagnetic and geological studies on Early Permian of the Yili and Junggar blocks are needed to better constrain the timing of relative motions as well as the mechanism of such tectonics.

6. Conclusions

This first paleomagnetic study is performed on sedimentary and volcanic rocks from the Yili Block. Magnetic mineralogical analyses show titanium-poor magnetite and hematite as the principal remanence carriers. Except the samples from the Axi area showing weak and unstable magnetic remanence, most of samples demagnetized by thermal and AF techniques demonstrate both viscous and stable components, the former gives a magnetic direction close to PEF and the latter presents characteristic remanent magnetization. The reversal polarity is exhaustively obtained from these Early and Late Carboniferous rocks and Late Permian red beds. A general re-magnetization of Early Carboniferous rocks has been observed due to the Late Carboniferous Yili arc magmatism. Two paleomagnetic poles of Late Carboniferous and Late Permian ages for the Yili Block are calculated from stable directions. Keeping in mind the important uncertainties, comparisons of both poles to the available coeval poles of Tarim, Junggar and Siberia indicate that (1) the consistency of poles from Yili and Junggar implies no or small relative motion between them since the Late Carboniferous; (2) no significant or small relative latitudinal movement occurred between these 4 blocks since Late Carboniferous; (3) 46.2°±15.1° and 31.6°±15.1° counterclockwise rotations of the Yili–Junggar blocks with respect to Tarim and Siberia, respectively, took place from Late Carboniferous to Late Permian. These rotations correspond to the eastward motions of Yili–Junggar Block with respect to Tarim (1160±380 km) along the dextral strike–slip faults in the Tianshan Belt and to Siberia (670±320 km) along the left-lateral Erqishi Fault in the Altay belt. These conclusions are supported by both field structural and kinematic observations as well as geochronologic studies in these tectonic zones.

Acknowledgement

This study has been supported by the National Basic Research Program of China (973 Programs) (Nos. 2007CB411301 and 2001CB409804) and French–Chinese Advanced Research Program (PRA T05-02, Y. CHEN & Q.C. WANG). French Embassy in Beijing is appreciated for financing part of research of the first author in France. Constructive suggestions provided by an anonymous reviewer and the editors have significantly improved the original manuscript.

References

Allen, M.B., Sengör, A.M.C., Natal'in, B.A., 1995. Junggar, Turfan and Alakol basins as Late Permian to ?Early Triassic extensional structures in a sinistral shear zone in the Altaid orogenic collage, Central Asia. J. Geol. Soc. (Lond.) 152, 327–338.

Allen, M.B., Windley, B.F., Zhang, C., 1992. Paleozoic collisional tectonics and magmatism of the Chinese Tien Shan, Central Asia. Tectonophysics 220, 89–115.

Avouac, J.P., Tapponnier, P., Bai, M., You, H., Wang, G., 1993. Active thrusting and folding along the northern Tien Shan and Late Cenozoic rotation of the Tarim relative to Dzungaria and Kazakhstan. J. Geophys. Res. 98 (B4), 6755–6804.

Bai, Y.H., Cheng, G.L., Sun, Q.G., Sun, Y.H., Li, Y.G., Dong, Y.J., Sun, D.J., 1987. Late Paleozoic polar wander path for the Tarim platform and its tectonic significance. Tectonophysics 139, 145–153.

Bazhenov, M.L., Burtman, V.S., Dvorova, A.V., 1999. Permian paleomagnetism of the Tien Shan fold belt, Central Asia: Post-collisional rotation and deformation. Tectonophysics 312 (2–4), 303–329.

Bazhenov, L.M., Chauvin, A., Audibert, M., Levashova, N.M., 1993. Permian and Triasic paleomagnetism of the southwestern Tien Shan: timing and mode of tectonic rotations. Earth Planet. Sci. Lett. 118, 195–212.

Bazhenov, L.M., Collins, A.Q., Degtyarev, K.E., Levashova, N.M., Mikolaichuk, A.V., Pavlov, V.E., Van der Voo, R., 2003. Paleozoic northward drift of the North Tianshan (Central Asia) as revealed by Ordovician and Carboniferous paleomagmatism. Tectonophysics 366, 113–141.

Burchfiel, B.C., Brown, E.T., Deng, Q.D., Feng, X.Y., Li, J., Molnar, P., Shi, J.B., Wu, Z.M., You, H.C., 1999. Crustal shortening on the Margins of the Tien Shan, Xinjiang, China. Int. Geol. Rev. 41, 665–700.

Burtman, V.S., 1975. Structural geology of variscan Tien Shan, USSR. Am. J. Sci. 275 (A), 157–186.

Charreau, J., Chen, Y., Gilder, S., Dominguez, S., Avouac, J.P., Sen, S., Sun, D.J., Li, Y.A., Wang, W.M., 2005. Magnetostratigraphy and rock magnetism of the Neogene Kuitun He section (northwest China): implications for Late Cenozoic uplift of the Tianshan mountains. Earth Planet. Sci. Lett. 230 (1–2), 177–192.

Chen, Y., Cogné, J.P., Courtillot, V., 1992. New Cretaceous paleomagnetic poles from the Tarim Basin, Northwestern China. Earth Planet. Sci. Lett. 114, 17–38.

Chen, Y., Courtillot, V., Cogné, J.P., Besse, J., Yang, Z., Enkin, R., 1993. The configuration of Asia prior to the collision of India: Cretaceous paleomagnetic constraints. J. Geophys. Res. 98, 21 927–21 941.

Chen, Y.B., Hu, A.Q., Zhang, G.X., Zhang, Q.F., 2000. Zircon U–Pb age of granitic gneiss on Duku highway in western Tianshan of China and its geological implications. Chin. Sci. Bull. 45 (7), 649–653 (in Chinese with English abstract).

Chen, C.M., Lu, H.F., Jia, D., Cai, D.S., Wu, S.M., 1999. Closing history of the southern Tianshan oceanic basin, western China: an oblique collisional orogeny. Tectonophysics 302, 23–40.

Cheng, G.L., Bai, Y.H., Li, Y.A., 1983. Paleomagnetism of Lower Permian in the Wushi–Aksu area of Xinjiang. Seismol.Geol. 5 (4), 12 (In Chinese).

Cogné, J.P., 2003. A MacintoshTM application for treating paleomagnetic data and making plate reconstructions. Geochem. Geophys. Geosyst. 4 (1). doi:10.1029/2001GC000227.

Coleman, R.G., 1989. Continental growth of northwest China. Tectonics 8 (3), 621–635.

Enkin, R.J., 2003. The direction–correction tilt test: an all-purpose tilt/fold test for paleomagnetic studies. Earth Planet. Sci. Lett. 212, 151–166.

Enkin, R.J., Chen, Y., Courtillot, V., Besse, J., Xing, L., Zhang, Z., Zhuang, Z., Zhang, J., 1991. A Lower Cretaceous pole from South China and the Mesozoic hairpin turn of the Eurasian apparent polar wander path. J. Geophys. Res 96, 4007–4028.

Fang, D.J., Chen, H.L., Jin, G.H., Guo, Y.B., Wang, Z.L., Tan, X.D., Yin, S.H., 1990. Late Paleozoic and Mesozoic paleomagnetism and tectonic evolution of Tarim terrane. In: Wiley, T.J., Howell, D.G., Wong, F.L. (Eds.), Terrane analysis of China and the Pacific rim, Houston (USA), Circum-Pacific Council for Energy and Mineral Resources. Earth Sci. Ser., vol. 13, pp. 251–255.

Fang, D.J., Jin, G.H., Jiang, L.P., Wang, P.Y., Wang, Z.L., 1996. Paleozoic paleomagnetic results from Tarim basin and their tectonic implication. Acta Geophys. Sin. 39 (4), 522–531 (in Chinese).

Fisher, R., 1953. Dispersion on a sphere. Proc. R. Soc. London, Ser. A 217, 295–305.

Gao, J., Li, M.S., Xiao, X.C., Tang, Y.Q., He, G.Q., 1998. Paleozoic tectonic evolution of the Tianshan orogen, northwestern China. Tectonophysics 287, 213–231.

Gilder, S., Zhao, X.X., Coe, R.S., Meng, Z., Courtillot, V., Besse, J., 1996. Paleomagnetism and tectonics of the southern Tarim basin, northwestern China. J. Geophys. Res. 101, 22 015–22 031.

Harkand, F., Cogné, J.P., Kravchinsky, V., 2005. A new Late Cretaceous paleomagnetic pole for the west of Amuria block (Khurmen Uul, Mongolia). Earth Planet. Sci. Lett. 236, 359–373.

Hounslow, M.W., Davydov, V.I., Klootwijk, C.T., Turner, P., 2004. Magnetostratigraphy of the Carboniferous: a review and future prospects. Newsl. Carbonifer. Stratigr. 22, 35–40.

Kirschvink, J.L., 1980. The least squares line and the analysis of paleoamgnetic data. Geophys. J. R. Astron. Soc. 62, 699–718.

Laurent-Charvet, S., Charvet, J., Monie, P., Shu, L.S., 2003. Late Paleozoic strike–slip shear zones in eastern Central Asia (NW China): new structural and geochronological data. Tectonics 22 (2), 1099–1101.

Laurent-Charvet, S., Charvet, J., Shu, L.S., Ma, R.S., Lu, H.F., 2002. Palaeozoic late collisional strike–slip deformations in Tianshan and Altay, eastern Xinjiang, NW China. Terra Nova 14 (4), 249–256.

Li, Y.P., McWilliams, M., Cox, A., Sharps, R., Li, Y.A., Gao, Z.J., Zhang, Z.K., Zhai, Y.J., 1988. Late Permian paleomagnetic pole from dikes of the Tarim craton, China. Geology 16, 275–278.

Li, Y.P., Sharps, R., McWilliams, M., Li, Y.G., Li, Q., Zhang, W., 1991. Late Paleozoic Paleomagnetic results from the Junggar block, Northwestern China. J. Geophys. Res. 96, 16 047–16 060.

Li, Y.P., Sharps, R., McWilliams, M., Nur, A., Li, Y.G., Li, Q., Zhang, W., 1989. Paleomagnetic results from Late Paleozoic dikes from the northwestern Junggar block, Northwestern China. Earth Planet. Sci. Lett. 94, 123–130.

Li, Y.J., Sun, L.D., Wu, H.R., Zhang, G.Y., Wang, G.L., Huang, Z.B., 2005. Permo-Carboniferous radiolarians from the Wupata'erkan group, Western South Tianshan, Xinjiang, China. Acta Geol. Sin. 79 (1), 16–23.

Li, Y.J., Wang, Z.M., Wu, H.R., Huang, Z.B., Tan, Z.J., Luo, J.C., 2002. Discovery of radiolarian fossils from the Aiketik group at the western end of the South Tianshan Mountains of China and its implications. Acta Geol. Sin. 76 (2), 146–154.

McFadden, P.L., Ma, X.H., McElhinny, M.W., Zhang, Z.K., 1988. Permo-Triassic magnetostratigraphy in China: northern Tarim. Earth Planet. Sci. Lett. 87, 152–160.

Meng, Z., 1991. Palaeomagnetic study of Upper Palaeozoic erathem along the southwestern margin of Tarim block, China. Acta Sedimentol. Sin. 9, 105–109 (in Chinese with English abstract).

Meng, Z., Zheng, J., 1990. Palaeomagnetic investigations of the Apparent Polar Wander path of Tarim and relative motions between sub-tectonic units. In: Zhou, Q., Zheng, J. (Eds.), Tectonic Synthesis of Tarim. Science Press, Beijing, pp. 50–87 (in Chinese with English abstract).

Nie, S.Y., Rowley, D.B., Van der Voo, R., Li, M.S., 1993. Paleomagnetism of Late Paleozoic rocks in the Tianshan, Northwestern China. Tectonics 12, 568–579.

Sengör, A.M.C., Natal'in, B.A., 1996. Palaeotectonics of Asia: Fragments of a synthesis. In: Yin, A., Harrison, M. (Eds.), The tectonic evolution of Asia, Rubey Colloquium. Cambridge University Press, Cambridge, pp. 486–640.

Sengör, A.M.C., Natal'in, B.A., Burtman, V.S., 1993. Evolution of the Altaid tectonic collage and Paleozoic crust growth in Eurasia. Nature 364, 299–307.

Sharps, R., Li, Y.P., McWilliams, M., Li, Y.G., 1992. Paleomagnetic investigation of Upper Permian sediments in the South Junggar Basin, China. J. Geophys. Res. 97, 1753–1765.

Shi, Y.S., Lu, H.F., Jia, D., Howell, D.G., 1994. Paleozoic plate tectonic evolution of the Tarim and western Tianshan Regions, Western China. Int. Geol. Rev. 36, 1058–1066.

Shu, L.S., Charvet, J., Guo, L.Z., Lu, H.F., Laurent-Charvet, S., 1999. A large-scale Palaeozoic dextral ductile strike–slip zone: the Aqqikkudug–Weiya zone along the northern margin of the Central Tianshan belt, Xinjiang, NW China. Acta Geol. Sin. 73 (2), 148–162.

Shu, L.S., Charvet, J., Lu, H.F., Laurent-Charvet, S., 2002. Paleozoic accretion–collision events and kinematics of ductile deformation in the central-southern Tianshan Belt, China. Acta Geol. Sin. 76 (3), 308–323.

Shu, L.S., Lu, H.F., Charvet, J., Laurent-Charvet, S., Yin, D.H., 2000. Paleozoic accretionary terranes in Northern Tianshan, NW China. Chin. Geochem. 19 (3), 193–202.

Shu, L.S., Wang, B., Yang, F., Lu, H.F., Charvet, J., Laurent-Charvet, S., 2003. Polyphase Tectonic Events and Mesozoic–Cenozoic Basin-

Range Coupling in the Chinese Tianshan belt. Acta Geol. Sin. 77 (4), 457–467.

Shu, L.S., Zhu, W.B., Wang, B., Faure, M., Charvet, J., Cluzel, D., 2005. The post-collision intracontinental rifting and olistostrome on the southern slope of Bogda Mountains, Xinjiang. Acta Petrol. Sin. 21 (1), 25–36 (in Chinese with English abstract).

Tapponnier, P., Molnar, P., 1979. Active faulting and Cenozoic tectonics of the Tienshan, Mongolia and Baykal regions. J. Geophys. Res. 84, 3425–3459.

Van der Voo, R., 1993. Paleomagnetism of the Atlantic, Tethys and Iapetus Oceans. Cambridge University Press, Cambridge.

Wang, B., Faure, M., Cluzel, D., Shu, L.S., Charvet, J., Meffre, S., 2006. Late Paleozoic tectonic evolution of the northern West Tianshan, NW China. Geodin. Acta 19 (3–4), 237–247.

Wang, B., Shu, L.S., Cluzel, D., Faure, M., Charvet, J., 2007. Geochemical Constraints on Carboniferous Volcanic rocks of Yili Block (Xinjiang, NW China); implication on tectonic evolution of Western Tianshan. J. Asian Earth Sci. 29, 148–159.

Wang, B., Faure, M., Shu, L.S., de Jong, K., Cluzel, D., Charvet, J., Meffre, S., Ruffet, G., Tectonics of the Yili Block in the southern part of the Western Chinese Tianshan, and its Paleozoic geodynamic evolution, Tectonics, in review.

Windley, B.F., Allen, M.B., Zhang, C., Zhao, Z.Y., Wang, G.R., 1990. Paleozoic accretion and Cenozoic redeformation of the Chinese Tien Shan range, Central Asia. Geology 18, 128–131.

XBGMR (Xinjiang Bureau of Geology and Mineralogy Resources), Geological map (scale 1:200000), Zhaosu sheet (K-44-10), 1979a.

XBGMR, Geological map (scale 1:200000), Gongliu sheet (K-44-5), 1979b.

XBGMR, Geological map (scale 1:200000), Xinyuan sheet (K-44-10), 1975.

XBGMR, Regional geology of Xinjiang Uygur Autonomy Region. Geology Publishing House, Beijing (in Chinese with English abstract).

XBGMR, Geological map (scale 1:200000), Sailimuhu sheet (K-44-34), 1988.

XBGMR, Geological map (scale 1:200000), Tuokuzi, Kumalak sheet (K-45-1), 1973.

Xia, L.Q., Xu, X.Y., Xia, Z.C., Li, X.M., Ma, Z.P., Wang, L.S., 2004. Petrogenesis of Carboniferous rift-related volcanic rocks in the Tianshan, northwestern China. Bull. Geol. Soc. Am. 116 (3–4), 419–433.

Yin, A., Nie, S.Y., 1996. A Phanerozoic palinspastic reconstruction of China and its neighboring regions. In: Yin, A., Harrison, M. (Eds.), The Tectonic Evolution of Asia, Rubey Colloquium. Cambridge University Press, Cambridge, pp. 442–485.

Zhai, Y.J., Zhang, Z.K., Li, Y.P., Li, Q., Li, Y., McWilliams, M., Cox, A., Sharps, R., 1988. A study of Upper Carboniferous paleomagnetism for the Tarim block. Geosciences 2, 43–56.

Zhao, J.M., Liu, G.D., Lu, Z.X., Zhang, X.K., Zhao, G.Z., 2003. Lithospheric structure and dynamic processes of the Tianshan orogenic belt and the Junggar basin. Tectonophysics 376, 199–239.

Zhou, D., Graham, S.A., Chang, E.Z., Wang, B.Y., Hacker, B., 2001. Paleozoic tectonic amalgamation of the Chinese Tianshan: Evidence from a transect along the Dushanzi–Kuqa highway. In: Hendrix, M.S., Davis, G.A. (Eds.), Paleozoic and Mesozoic tectonic evolution of central Asia: from continental assembly to intracontinental deformation, Boulder, Colorado. Geol. Soc. Am. Mem., vol. 194, pp. 23–46.

Zhu, Y.F., Zhang, L.F., Gu, L.B., Guo, X., Zhou, J., 2005. The zircon SHRIMP chronology and trace element geochemistry of the Carboniferous volcanic rocks in western Tianshan Mountains. Chin. Sci. Bull. 50 (19), 2201–2212 (in Chinese with English abstract).

Zijderveld, J.D.A., 1967. A.C. demagnetization of rocks: analysis of results. In: Collinson, D.W., Creer, K.M., Runcorn, S.K. (Eds.), Methods on Paleomagnetism. Elsevier, New York, pp. 245–286.